



Review

Scandium-44: Diagnostic Feasibility in Tumor-Related Angiogenesis

György Trencsényi and Zita Képes *

Division of Nuclear Medicine and Translational Imaging, Department of Medical Imaging, Faculty of Medicine, University of Debrecen, Nagyerdei St. 98, H-4032 Debrecen, Hungary; trencsenyi.gyorgy@med.unideb.hu

* Correspondence: kepes.zita@med.unideb.hu

Abstract: Angiogenesis-related cell-surface molecules, including integrins, aminopeptidase N, vascular endothelial growth factor, and gastrin-releasing peptide receptor (GRPR), play a crucial role in tumour formation. Radiolabelled imaging probes targeting angiogenic biomarkers serve as valuable vectors in tumour identification. Nowadays, there is a growing interest in novel radionuclides other than gallium-68 (^{68}Ga) or copper-64 (^{64}Cu) to establish selective radiotracers for the imaging of tumour-associated neo-angiogenesis. Given its ideal decay characteristics (E_{β^+} average: 632 KeV) and a half-life ($T_{1/2} = 3.97$ h) that is well matched to the pharmacokinetic profile of small molecules targeting angiogenesis, scandium-44 (^{44}Sc) has gained meaningful attention as a promising radiometal for positron emission tomography (PET) imaging. More recently, intensive research has been centered around the investigation of ^{44}Sc -labelled angiogenesis-directed radiopharmaceuticals. Previous studies dealt with the evaluation of ^{44}Sc -appended $\alpha_v\beta_3$ integrin-affine Arg-Gly-Asp (RGD) tripeptides, GRPR-selective aminobenzoyl-bombesin analogue (AMBA), and hypoxia-associated nitroimidazole derivatives in the identification of various cancers using experimental tumour models. Given the tumour-related hypoxia- and angiogenesis-targeting capability of these PET probes, ^{44}Sc seems to be a strong competitor of the currently used positron emitters in radiotracer development. In this review, we summarize the preliminary preclinical achievements with ^{44}Sc -labelled angiogenesis-specific molecular probes.

Keywords: aminobenzoyl-bombesin analogue (AMBA); aminopeptidase N (APN/CD13); angiogenesis; carcinogenesis; gastrin-releasing peptide receptor (GRPR); integrin; nitroimidazole; positron emission tomography (PET); Arg-Gly-Asp (RGD); scandium-44 (^{44}Sc)



Citation: Trencsényi, G.; Képes, Z. Scandium-44: Diagnostic Feasibility in Tumor-Related Angiogenesis. *Int. J. Mol. Sci.* **2023**, *24*, 7400. <https://doi.org/10.3390/ijms24087400>

Academic Editor: Efstratios Stratikos

Received: 15 March 2023

Revised: 12 April 2023

Accepted: 13 April 2023

Published: 17 April 2023



Copyright: © 2023 by the authors. Licensee MDPI, Basel, Switzerland. This article is an open access article distributed under the terms and conditions of the Creative Commons Attribution (CC BY) license (<https://creativecommons.org/licenses/by/4.0/>).

1. Introduction

1.1. Tumour-Related Angiogenesis

The formation of new blood vessels from pre-existing ones—denoted as angiogenesis—is required for tumour maintenance and development as well as for metastasis formation [1,2]. Angiogenesis is regulated by a delicate balance between a host of pro-angiogenic and antiangiogenic factors [3]. Hence, intensive attention has been placed on the assessment of cancer-associated neovascularization [4,5]. Producing various angiogenic factors, proteases, heparanase, digestive enzymes, and chemotactic and stimulatory factors, tumour cells exert a direct effect on capillary endothelial cells, induce the assembly of activated immune cells, and trigger the activity of stromal cells; thus, they create a pro-angiogenic niche in the tumour microenvironment [2,6].

Given that angiogenesis/neo-angiogenesis has crucial role in tumour development, propagation, and metastatic spread, angiogenic biomarkers are recorded as promising candidates for tumour imaging [7]. Vascular endothelial growth factor (VEGF), platelet-derived growth factor (PDGF), fibroblast growth factor-2 (FGF-2), ephrins, $\alpha_v\beta_3$ integrins, aminopeptidase N (APN/CD13), fibronectin, nitroimidazole, matrix metalloproteinases, gastrin-releasing peptide receptor (GRPR), and E-selectin represent the most important angiogenic molecules [8]. The detection of angiogenesis-related markers makes timely tumour identification possible, and these biomolecules also serve as potential targets for

anti-tumour treatment and patient follow-up [1,9]. Anti-angiogenic drugs can inhibit tumour expansion and decelerate, delay, or even inhibit tumour augmentation and metastasis formation [10,11]. Therefore, angiogenesis-directed molecular probes may lay the basis of personalised cancer diagnostics and treatment.

Non-invasive positron emission tomography (PET) or positron emission tomography/computed tomography (PET/CT) are regarded as the mainstay diagnostic tools in the detection of primary tumours and pertinent metastases. Furthermore, PET can be a useful means of angiogenesis-targeted drug development, authorization, and dose estimation [8,12]. Several PET radionuclides have been used in angiogenesis-directed diagnostical settings, including fluoride-18 (^{18}F), gallium-68 (^{68}Ga), copper-64 (^{64}Cu), and even the gamma emitter indium-111 (^{111}In). Although scandium (Sc) radioisotopes were already recognized as valuable radiometals for isotope diagnostic use in the late 1990s, they have been set aside for almost 20 years [13].

1.2. Scandium-44 (^{44}Sc)

The following three radionuclides of Sc are well suited for either diagnostic or therapeutic applications: scandium-43 (^{43}Sc), scandium-44 (^{44}Sc), and scandium-47 (^{47}Sc) [14]. Positron emitters ^{43}Sc and ^{44}Sc are relevant diagnostic radiometals, whereas β^- -emitting ^{47}Sc is the therapeutic sister with accompanying γ rays for imaging purposes [15,16].

There are two major ways to produce ^{44}Sc . Via the proton irradiation of natural calcium or enriched ^{44}Ca targets (through a $^{44}\text{Ca}(p,n)^{44}\text{Sc}$ nuclear reaction), the production of ^{44}Sc can be easily obtained by applying low-energy cyclotrons [17–19]. Cyclotron-based production provides outstanding radiochemical yield (RCY) and radiochemical purity (RCP) for clinical applications [18,20]. Of note, ^{44}Sc production via applying a cyclotron has been confirmed to be economically viable [17]. Although ^{44}Sc can also be eluted from titanium-44/scandium-44 ($^{44}\text{Ti}/^{44}\text{Sc}$) generator systems, the radioactive-waste handling of long-lived ^{44}Ti (62 ± 2 years) makes this approach challenging [21–23]. In addition, the demanding production of ^{44}Ti implies another obstacle regarding the routine usage of $^{44}\text{Ti}/^{44}\text{Sc}$ generators [17,24]. Difficulties around the production of ^{44}Sc may underpin why this radiometal came to the focus of exhaustive investigation as a potential labelling isotope so late.

^{44}Sc , with physical properties of $T_{1/2}$: 3.97 h (lately reported as 4.04 h), E_{β^+} average: 632 KeV, E_{β^+} mean: 0.63 MeV, and I:94.3%, has begun to emerge as a radiometal of particular interest in imaging, dosimetry, and treatment follow-up [20,25,26]. Positron emitter ^{44}Sc also has a gamma co-emission of 1157 keV (99.9%), which may limit the radioactive dose that can be injected into patients [26]. However, this high-energy gamma radiation made the radiometal a precious candidate for the novel $\beta + \gamma$ coincidence PET imaging [27]. Since the positron energy of the applied PET radionuclide is inversely proportional to the resolution of the reconstructed image, better spatial-image resolution and better quality could be obtained with ^{44}Sc relative to other radiometals—for example, ^{68}Ga (^{68}Ga : E_{β^+} max: 1.9 MeV and E_{β^+} mean: 0.89 MeV vs. ^{44}Sc : E_{β^+} max: 1474 KeV and E_{β^+} mean: 0.63 MeV) [28–30]. These advantageous physical characteristics together with its decay to nontoxic Ca make ^{44}Sc widely feasible in PET and PET/CT imaging [13,31]. Given its small ionic radius, the chemistry of ^{44}Sc is comparable to that of ^{68}Ga ; thus, ^{44}Sc could be applied in several fields, including dosimetry investigations in theranostic settings and in trafficking ligands with longer pharmacokinetics and subsequent requirements for longer imaging times (even 24 h post administration) [32,33].

Prior studies have already dealt with the investigation of the feasibility of ^{44}Sc in pre-therapeutic dosimetry [34,35]. Khawar et al. published a paper indicating that the pharmacokinetics of [^{44}Sc]Sc-PSMA-617-based (PSMA (prostate-specific membrane antigen)) PET/CT imaging serves as a useful tool for the calculation of normal organ-absorbed doses and the maximum allowable activity in prostate-cancer patients prior to lutetium-177 (^{177}Lu)-labelled PSMA-617 ([^{177}Lu]Lu-PSMA-617) radiotherapy [36]. Pioneering clinical studies further strengthened the efficacy of ^{44}Sc -labelled somatostatin analogue [^{44}Sc]Sc-DOTATOC and [^{44}Sc]Sc-PSMA-617 as valuable radiotracers in dosimetry settings [35].

Delayed acquisition granted by the longer half-life of ^{44}Sc enables better pre-therapeutic dosimetry for [^{177}Lu]/Lu-PSMA-617 radiotherapy [34,37]. Clinical successes in the treatment of leukaemia, non-Hodgkin lymphoma, malignant melanoma, urinary bladder cancer, glioma, neuroendocrine tumours, and prostate cancer with alpha emitter bismuth-213 (^{213}Bi)- and actinium-225 (^{225}Ac)-linked radiopharmaceuticals project that these isotopes could also benefit from dosimetry estimations based on ^{44}Sc [38]. Moreover, in the long run, other radionuclides, such as yttrium-90 (^{90}Y), ioide-131 (^{131}I), strontium-90 (^{90}Sr), and phosphorus-32 (^{32}P) may be potential candidates for theranostic applications. Although preclinical research findings are available on radiation-absorbed doses from ^{47}Sc , the limited availability of the radiometal hampers its usage as a potential radiotherapeutic agent [39].

Similar to ^{68}Ga , ^{44}Sc is also able to form thermodynamically stable complexes with chelator DOTA (1,4,7,10-terazacyclododecane- $\text{N},\text{N}',\text{N}'',\text{N}'''$ -teraacetic acid) [40,41]. In addition to this, ^{44}Sc seems superior to ^{68}Ga in several facets. Given its longer half-life ($T_{1/2}$ ^{44}Sc : 3.97 h vs. $T_{1/2}$ ^{68}Ga : 68 min) and cyclotron-dependent extensive synthesis, ^{44}Sc can be easily shipped to remote nuclear medical facilities. This contributes not only to the wider distribution of the radioisotope but also to the accomplishment of protein- or antibody-based PET studies with lengthened examination times [42]. Furthermore, radiopharmaceuticals with longer pharmacokinetic characteristics can also be proposed due to the longer half-life of the radiometal [17]. Moreover, the pharmacokinetic properties of ^{44}Sc -appended imaging probes are largely comparable to those of the ^{68}Ga -labelled counterparts [43]. The nearly four-hour half-life of ^{44}Sc could be easily fitted to the pharmacokinetics of several targeting molecules, including peptides, antibodies, or their fragments, as well as oligonucleotides, which makes facile radiopharmaceutical synthesis possible [13,17]. Additionally, long-lived ^{44}Sc favours delayed imaging and the achievement of appropriate tumour-to-background (T/M) ratios. The time of imaging is of critical importance from the point of view of patient management and the scheduling of examinations. Therefore, the use of ^{44}Sc -labelled radiopharmaceuticals would contribute to the establishment of a fluent workflow.

^{44}Sc -labelled PET radiopharmaceuticals could even be appropriate for intraoperative radio-guided surgery, including the detection of lymphatic metastases at later time points post injection [32]. Consequently, ^{44}Sc -based PET probes could stand out as valuable imaging agents. ^{47}Sc ($T_{1/2}$ = 3.35 days)—the therapeutic match of ^{44}Sc —emits a β^- radiation of a maximum energy of 0.600 MeV (31.6%) and 0.439 MeV (68.4%), which could be exploited in targeted radiotherapy [33,44]. Therefore, $^{44}\text{Sc}/^{47}\text{Sc}$ has exquisite potential as a radio-theranostic pair in PET diagnostics and in therapeutic settings [33,45]. Besides ^{44}Sc and ^{47}Sc , scandium-43 (^{43}Sc) is another significant member of the group of Sc isotopes. Investigating the quantitative capabilities of $^{43}\text{Sc}/^{44}\text{Sc}$ and comparing it to ^{18}F and ^{68}Ga , Lima et al. published a paper indicating that the application of radiotracers labelled with the mixture of $^{43}\text{Sc}/^{44}\text{Sc}$ may be beneficial in clinical fields [46]. The findings of their phantom study proved that precise, quantitative PET/CT could be obtained by applying commercial PET systems [46]. Given that ^{43}Sc does not have high-energy gamma emission, the use of $^{43}\text{Sc}/^{44}\text{Sc}$ could be especially important in terms of overcoming the limitation of ^{44}Sc derived from gamma radiation. These favourable features propelled both preclinical and clinical investigations with ^{44}Sc down new lines. Some experiments have been spawned to focus on the evaluation of the clinical feasibility of ^{44}Sc -labelled molecules at a translational level as well as the comparison of ^{44}Sc with other widely used radionuclides, such as ^{68}Ga and ^{64}Cu [47].

1.3. PET Radioisotopes Other Than Scandium-44 (^{44}Sc)

The optimal short half-life (109.8 min) and the high positron abundance ($\beta \geq 97\%$) of ^{18}F made it the most commonly used radioisotope for the labelling of PET biomolecules [48]. Positron emitter ^{18}F possesses a relatively low positron energy ($E_{\text{max}} = 0.635$ MeV and $E_{\text{mean}} = 0.250$ MeV) and a short positron range within the tissue (maximum of 2.3 mm) [49,50]. These nuclear properties ensure ideal image quality and high spatial resolution obtained with

^{18}F -labelled tracers [51]. The 109.8 min-long half-life is beneficial for synthesis procedures as well as for the performance of examinations of a few hours [51]. Owing to the short longevity, ^{18}F -labelled radiopharmaceuticals can be safely administered without an increased risk of excess radiation. Moreover, another advantage is the facile cyclotron-based production, which provides immense quantities of the isotope at high specific activity [51]. Although a cyclotron is required to produce the radiometal, its decay characteristics make the distribution of ^{18}F - and ^{18}F -labelled radiotracers to distant nuclear medical laboratories without an on-site cyclotron possible. Even though ^{18}F is well suited for the labelling of a wide range of small and medium-sized molecules, the radiolabelling of peptides with ^{18}F is still cumbersome [51]. Hence, different isotopes have come into focus that address some of the difficulties associated with ^{18}F -based radiotracers.

Up to now, the favourable physical characteristics of ^{68}Ga and ^{64}Cu made them attractive for the radiolabelling of a broad set of molecules. Currently, ^{68}Ga -labelled PET radiopharmaceuticals are applied most frequently for labelling purposes of radiometal-based PET tracers. The short-lived positron emitter ^{68}Ga ($T_{1/2}$: 67.71 min \approx 68 min, $E_{\beta^+ \text{ average}}$: 830 KeV, maximum β^+ energy: 1.92 MeV, I_{β^+} : 89%, E_{γ} : 1077 KeV, I_{γ} : 3.2%) can be obtained from a germanium-68/gallium-68 ($^{68}\text{Ge}/^{68}\text{Ga}$)-generator system [52,53]. With such physical properties, decay characteristics, and easy accessibility from an on-site $^{68}\text{Ge}/^{68}\text{Ga}$ generator, ^{68}Ga has emerged as the mainstay PET-imaging radiometal [32,52,54]. Since the radiosynthesis of peptides—complexed with different macrocyclic ligands—with ^{68}Ga is easy to perform, the use of ^{68}Ga is effective in imaging settings [55]. ^{68}Ga -labelled DOTA-conjugated somatostatin analogues (SSTR), including DOTATOC, DOTATATE, and DOTANOC, meant a substantial step forward in the imaging of SSTR-positive neuroendocrine tumours [33].

The short half-life and related transport challenges, however, may limit the widespread implementation of ^{68}Ga into clinical and preclinical settings. Owing to the short longevity of the radiometal, radiolabelling procedures are only possible in laboratories equipped with in-house $^{68}\text{Ge}/^{68}\text{Ga}$ -generator systems. In addition, due to its short half-life, ^{68}Ga -labelling can be applied solely in case of small molecules and peptides featured with a rapid pharmacokinetic profile [17,56]. Furthermore, ^{68}Ga -labelling is only suitable for PET examinations of relatively short duration. Because of the breakthrough of ^{68}Ge and sorbent material, the purification and concentration of ^{68}Ga is warranted following elution, which could also restrict its applicability in routine diagnostic usage [57]. Image noise associated with the elevated positron energy of the radionuclide constitutes another shortcoming of ^{68}Ga imaging [32]. These facts render ^{68}Ga -labelled radiotracers of limited attractiveness for centralized distribution.

The application of ^{64}Cu may bridge the limitations derived from ^{68}Ga -associated imaging. Given its longer half-life ($T_{1/2}$: 12.7 h) and generator-independent production, the use of ^{64}Cu (β^+ emission, $E_{\text{average}} = 278$ keV, abundance: 19%) seems to be economically more viable for PET imaging [58,59]. Due to its longer-lived nature, the easy transport to distant laboratories without an on-site cyclotron facilitates the integration of ^{64}Cu -appended radiopharmaceuticals into diagnostics. Moreover, the 12.7 h half-life of the radiometal can be easily tailored to biomarker-targeting small and large molecules, peptides, antibodies, and nanomolecules with prolonged elimination kinetics [60]. Additionally, its longer half-life makes ^{64}Cu -based radiochemical procedures facile [60]. The coordination chemistry of the radiometal enables complexation with various chelating agents, which further supports the frictionless performance of radiolabelling [60]. Therefore, ^{64}Cu is extremely useful in the establishment of a broad set of radiotracers for diagnostic purposes. However, the use of ^{64}Cu is not without shortcomings. Its concomitant β^- emission ($\beta^- = 39.0\%$, $E = 190.2$ keV) and relatively low positron-branching ratio (17.6%) mean a meaningful extra radiation danger for patients [58,61,62]. Furthermore, in case of complexation, chelators must be customized to the complex redox chemistry of ^{64}Cu [54].

Beyond ^{44}Sc , the use of zirconium-89 (^{89}Zr) has also been exhaustively investigated in PET imaging [63]. Given its favourable decay half-life ($T_{1/2} = 3.3$ days; 78.4 h), appropriate

radiochemistry, and the accessibility of different chelating agents for complexation with the radioisotope, ^{89}Zr is welcomed for the radiolabelling of PET-based imaging molecules [63]. The relatively long half-life of the radiometal could be easily adjusted to the pharmacokinetic profile of monoclonal antibodies (mAbs); therefore, ^{89}Zr seems to be well suited for the radiolabelling of mAbs and for PET immunoimaging applications [63–65]. Several mAbs, including anti-human epidermal growth factor receptor 2 (HER2) trastuzumab, anti-epidermal growth factor receptor (EGFR) mAb cetuximab, anti-PSMA mAb J591, and anti-vascular endothelial growth factor (VEGF) bevacizumab, were successfully labelled with ^{89}Zr for the PET imaging of breast cancer, squamous-cell carcinoma, prostate tumours, and ovarian tumours, respectively, at both preclinical and clinical levels [66–69].

Due to their decay characteristics (positron emission: E_{max} and E_{average} , 897 keV and 396.9 keV, respectively), PET images obtained with ^{89}Zr -labelled compounds are of adequate spatial resolution [70–72]. However, similar to ^{44}Sc , ^{89}Zr has spontaneous high-energy gamma radiation of 908.97 keV, which accounts for a major drawback of its usage [70]. Although the concomitant gamma radiation does not influence either the quality or the quantification of the PET scans, it needs to be taken into account when patient doses are determined [73,74]. Another potential disadvantage could be the limited availability of the radiometal [63].

Taking the abovementioned facts into account, ^{44}Sc may therefore be a valuable substitute for the currently applied ^{68}Ga and ^{64}Cu in the establishment of peptide-based targeted PET radiopharmaceuticals. In this review, we provide a comprehensive overview of the role of ^{44}Sc -labelled peptide-based radiopharmaceuticals in the molecular imaging of cancer-related angiogenesis (Figure 1). Table 1 summarises the preclinical studies with ^{44}Sc -labelled PET radiotracers that selectively target angiogenic biomarkers. In Table 2 the most important physical characteristics of the discussed PET radioisotopes are displayed.

AMBA: aminobenzoyl–bombesin analogue; APN/CD13: aminopeptidase N; BBN: bombesin; GRPR: gastrin-releasing peptide receptor; NGR: asparagine–glycine–arginine; PET: positron emission tomography; RGD: Arg–Gly–Asp; ^{44}Sc : scandium-44; ^{47}Sc : scandium-47.

AAZTA: (1,4-bis(carboxymethyl)-6-[bis(carboxymethyl)]amino-6-methylperhydro-1,4-diazepine) AMBA: aminobenzoyl–bombesin analogue; AR42J: rat exocrine pancreatic tumour; BBN: bombesin; BN: bombesin; c(RGD)₂: dimeric cyclic arginine–glycine–aspartic acid; c(RGDfK): cyclo(-Arg–Gly–Asp–d-Phe–Lys); DOTA: 1,4,7,10-terazacyclododecane–N,N',N'',N'''-teraacetic acid; ELISA: enzyme-linked immunosorbent assay; ^{68}Ga : gallium-68; GRPR: gastrin-releasing peptide receptor; HaCaT: human immortal keratinocyte; ^{125}I : iodine-125; KB: human epidermal carcinoma; NI: nitroimidazole; NODAGA: 1,4,7-triazacyclononane-1-glutaric acid-4,7-diacetic acid; NRP-1: neuropilin-1 co-receptor; PCa PC-3: prostate cancer; PET/CT: positron emission tomography/computed tomography; PET/MRI: positron emission tomography/magnetic resonance imaging; RGD: Arg–Gly–Asp; ^{44}Sc : scandium-44; SCID: severe combined immunodeficient; 4T1: mouse breast cancer; U87MG: human glioblastoma; VEGF: vascular endothelial growth factor.

Table 1. Preclinical studies with ^{44}Sc -labelled PET radiotracers.

Investigated Object	Investigated Phenomenon	Target Molecule	(Radio) Labelled Vector	Imaging Technique	Reference
PCa PC-3 and HaCaT cell lines	In vitro receptor-binding affinity utilizing in vitro blocking studies with BBN	GRPR	^{44}Sc Sc-NODAGA-AMBA and ^{68}Ga Ga-NODAGA-AMBA,	In vitro gamma counter measurements %ID/million cells units	[75]

Table 1. Cont.

Investigated Object	Investigated Phenomenon	Target Molecule	(Radio) Labelled Vector	Imaging Technique	Reference
PCa PC-3 tumor-bearing CB17 SCID mice and healthy control	In vitro and in vivo biodistribution pattern, tumor-targeting capability based on blocking experiments	GRPR	[⁴⁴ Sc]Sc-NODAGA-AMBA and [⁶⁸ Ga]Ga-NODAGA-AMBA	In vivo miniPET imaging, ex vivo radioactivity determination by gamma counter (%ID/g), in vivo and ex vivo blocking studies with BBN	[75]
PC-3 cell line	In vitro receptor-binding affinity with blocking studies applying [¹²⁵ I-Tyr ⁴]-BN	GRPR	^{nat} Sc-DOTA-BN[2-14]NH ₂ and ^{nat} Ga-DOTA-BN[2-14]NH ₂	Competitive displacement cell-binding assay	[33]
Healthy male Sprague-Dawley rats, male Copenhagen rats bearing androgen-independent Dunning R-3327-AT-1 prostate cancer tumour	In vivo and ex vivo organ distribution, GRPR-targeting ability applying blocking studies with BBN	GRPR	⁴⁴ Sc-DOTA-BN[2-14]NH ₂ and ⁶⁸ Ga-DOTA-BN[2-14]NH ₂	In vivo dynamic microPET imaging (in tumourous rats), ex vivo (in healthy rats) radioactivity calculations with a dose calibrator (% ID/g)	[33]
U87MG and AR42J tumour-bearing female athymic nude mice (CD-1 nude)	Evaluation of in vitro and in vivo behaviour, in vivo and ex vivo biodistribution	$\alpha_v\beta_3$ integrin	[⁴⁴ Sc]Sc-DOTA-RGD, [⁴⁴ Sc]Sc-NODAGA-RGD, [⁶⁸ Ga]Ga-DOTA-RGD, [⁶⁸ Ga]Ga-NODAGA-RGD	In vivo PET/CT acquisition, ex vivo gamma counting (%IA/g)	[76]
4T1 tumor-bearing BALB/c mice and healthy control	applicability of chelator AAZTA, in vivo biodistribution	$\alpha_v\beta_3$ integrin	⁴⁴ Sc ³⁺ , and ⁴⁴ Sc(AAZTA) ⁻ and ⁴⁴ Sc(CNAAZTA-c(RGDfK))	in vivo PET/MRI examinations	[77]
U87MG cells	In vitro receptor-binding affinity and specificity with blocking studies using ¹²⁵ I-Echistatin	$\alpha_v\beta_3$ integrin	cRGD, (cRGD) ₂ , and DOTA-(cRGD) ₂	In vitro competitive cell-binding assay, gamma counter-based detection of the tracer concentration	[17]
U87MG glioblastoma-bearing female athymic nude mice	Tumour-targeting competence, specificity applying in vivo and ex vivo receptor blocking with c(RGD) ₂ , in vivo and ex vivo biodistribution	$\alpha_v\beta_3$ integrin	[⁴⁴ Sc]Sc-DOTA-c(RGD) ₂	In vivo microPET/microCT imaging, ex vivo radioactivity determination (%ID/g)	[17]

Table 1. Cont.

Investigated Object	Investigated Phenomenon	Target Molecule	(Radio) Labelled Vector	Imaging Technique	Reference
CB17 SCID adult male mice bearing KB tumours and healthy control mice	Synthesis procedure, comparison of ^{44}Sc - and ^{68}Ga -labelled derivatives, in vivo and ex vivo biodistribution	Hypoxia	^{44}Sc [Sc-DO3AM-NI and ^{68}Ga]Ga-DO3AM-NI	In vivo PET/MRI studies, ex vivo radiopharmaceutical uptake measurement %ID/g	[78]
Pro-angiogenic VEGF-A ₁₆₅ /NRP-1 complex formation	Investigation of physicochemical properties and affinity for NRP-1	NRP-1	^{44}Sc - radiocompounds (^{44}Sc -1, ^{44}Sc -1bis, ^{44}Sc -2, ^{44}Sc -3):Sc-DOTA-Ahx-A7R (Sc-1), Lys(DOTA-Sc)-A7R (Sc-1bis), Lys(hArg)-Dab(Ahx-DOTA-Sc)-Pro-Arg (Sc-2) and DR7A-DLys(DOTA-Sc) (Sc-3)	Competitive ELISA test	[79]

Table 2. Physical characteristics of commonly used PET radionuclides.

	^{18}F	^{68}Ga	^{64}Cu	^{43}Sc	^{44}Sc	^{89}Zr
Half-life (h)	1.83	1.13	12.7	3.89	3.97	78.41
Decay method (%)	EC (3) β^+ (97)	EC (11.1) β^+ (88.9)	EC (43.9) β^+ (17.6) β^- (38.5)	EC (12) β^+ (88)	EC (5.7) β^+ (94.3)	EC (77.3) β^+ (22.7)
β^+ endpoint energy, keV (%)	633.5 (96.7%)	1899 (87.7) 822 (1.2)	653 (17.6)	1200 (70.9) 826 (17.2)	1474 (94.3)	902 (22.8)
Principal γ energies, keV (Abs.%)	511 (194)	511 (177.8) 1077 (3.2) 1261 (0.1) 1883 (0.1)	511 (35.2) 1346 (0.5)	372.8 (23)	511 (188.5) 1157 (99.9) 1499 (0.9)	511 (45.5) 909 (99.0) 1713 (0.7) 1745 (0.1)

EC: electron capture.

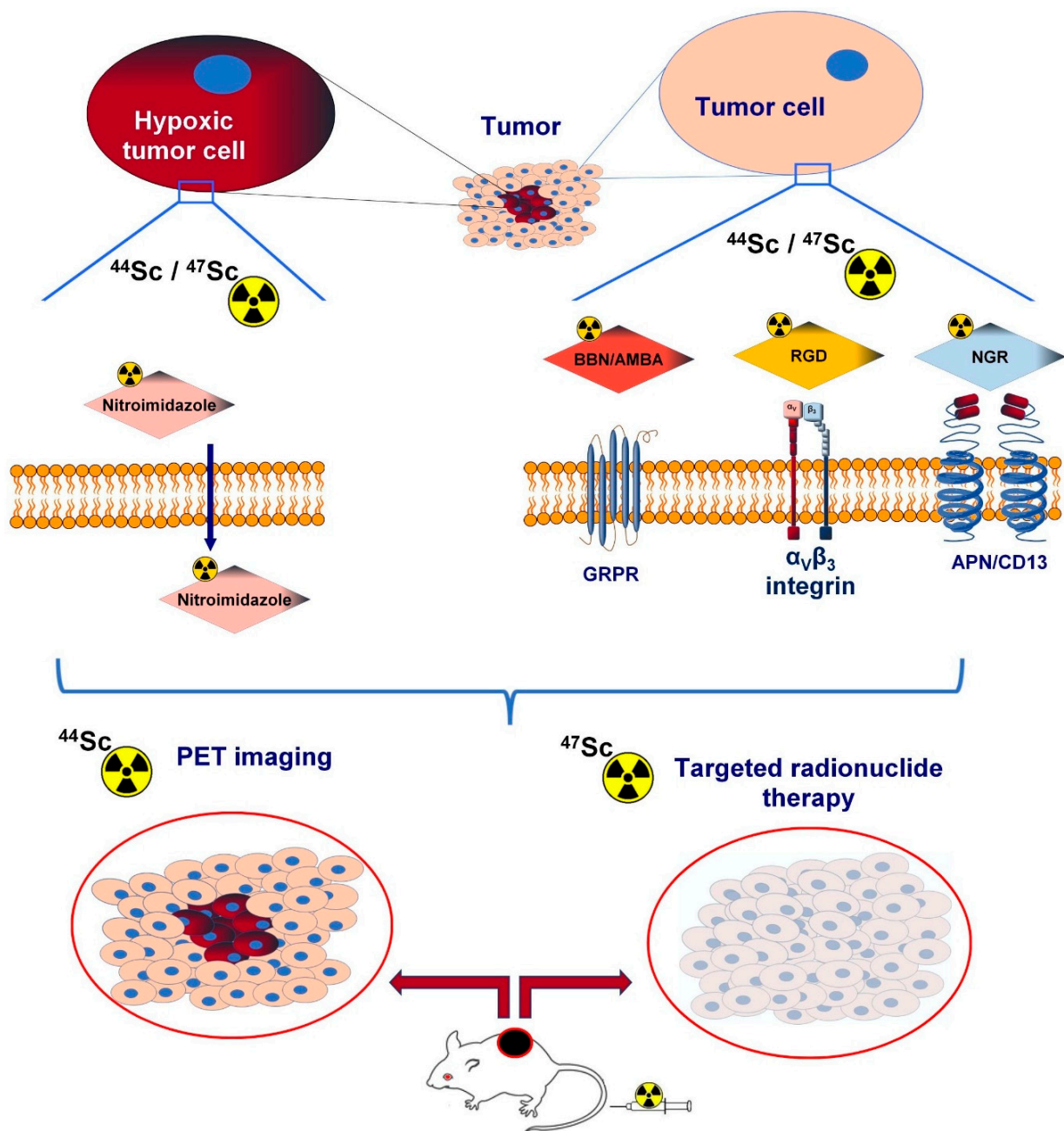


Figure 1. Sc^{44} - and Sc^{47} -labelled peptide-based radiopharmaceuticals in the molecular imaging and therapy of cancer-related angiogenesis.

2. Integrin $\alpha_v\beta_3$

$\alpha_v\beta_3$ integrin has a central role in angiogenesis, neovascularisation, tumour growth, and related metastatic spread [80]. Built up by noncovalently assembled α and β transmembrane subunits, the $\alpha_v\beta_3$ integrin heterodimer is able to adhere to a wide set of target molecules, including extracellular matrix (ECM) or soluble ligands and different cell-surface molecules [81,82]. The interaction of $\alpha_v\beta_3$ integrin with ECM proteins, fibroblast growth factor-2 (FGF2), metalloproteinase MMP-2, activated platelet-derived growth factor (PDGF), insulin, and vascular endothelial growth factor (VEGF) receptors favours cellular adhesion, cell proliferation, migration, and invasiveness, as well as the inhibition of apoptotic processes [83,84].

Since $\alpha_v\beta_3$ integrin is upregulated in a vast array of cancer cells, tumour endothelial cells, and new-born blood vessels, it is recorded as an impressive biomarker of angiogenesis in oncological tumour diagnostics [82]. In addition, the expression level of $\alpha_v\beta_3$ integrin correlates well with angiogenic activity, which makes the receptor suitable for the trafficking of antiangiogenic therapy.

Arg-Gly-Asp (RGD) tripeptides specifically bind to integrin receptors [85]. The affinity of an RGD sequence containing peptides to $\alpha_v\beta_3$ integrin has increased its attractiveness for the development of RGD-based PET and single-photon emission computed tomography (SPECT) radioindicators in the detection of tumour-associated angiogenesis. Intensive focus has been placed upon the evaluation of ^{18}F - and ^{68}Ga -labelled, integrin-targeted PET radiotracers such as [^{18}F]F-galacto-RGD, [^{18}F]F-fluciclatide, [^{18}F]F-RGD-K5, [^{18}F]F-FPPRGD2, [^{18}F]F-alfatide, [^{68}Ga]Ga-NOTA-RGD, and [^{68}Ga]Ga-NOTA-PRGD2 [85–92]. More recently, ^{44}Sc -based RGD radiopharmaceuticals have gained increasing interest for tumour-imaging scenarios.

Hernandez et al. used ^{44}Sc that was obtained from a cyclotron by the proton irradiation of natural Ca metal targets for the labelling of $\alpha_v\beta_3$ integrin-affine dimeric cyclic arginine-glycine-aspartic acid (cRGD)₂ to assess the peptide selectivity of [^{44}Sc]Sc-DOTA-c(RGD)₂ at both the in vivo and in vitro levels [17]. The tumour-targeting capability, the specificity, and the binding potential of this radioisotope were assessed in vitro, in vivo, and ex vivo by performing competitive-cell binding assay, small-animal PET examinations, receptor-blocking studies, and organ-distribution experiments. For the in vivo evaluation of the $\alpha_v\beta_3$ -targeting capacity of [^{44}Sc]Sc-DOTA-c(RGD)₂, U87MG human glioblastoma-bearing female athymic nude mice were intravenously (iv.) administrated with 5.5–7.4 MBq of the radiotracer and then underwent microPET/microCT acquisition at different time points (0.5, 2, and 4 h post injection). The $\alpha_v\beta_3$ integrin overexpression of the tumour cells and the vasculature of the U87MG experimental models is well established. In a bid to assess the $\alpha_v\beta_3$ selectivity of cRGD, (cRGD)₂, and DOTA-(cRGD)₂ in vitro, a competitive cell-binding assay was performed using integrin-targeting radioligand ^{125}I -echistatin. Moreover, in vivo and ex vivo receptor-blocking studies were further conducted with the simultaneous application of 3.7 MBq of [^{44}Sc]Sc-DOTA-c(RGD)₂ and 50 mg/kg (approximately 1 mg) of (cRGD)₂ to confirm receptor selectivity. During the competitive assays, continuously elevating amounts of cRGD, (cRGD)₂, and DOTA-(cRGD)₂ were administered to 1×10^5 U87MG cells that were pre-incubated with ^{125}I -echistatin. As part of the ex vivo experiments, the weight and radioactivity of the harvested major tissues and organs, the blood, and the tumour were measured. The tracer-uptake values were obtained as mean %ID/g \pm SD. Due to the significantly elevated tracer accumulation of the tumours, along with the negligible background activity, high-contrast PET images could be obtained at each investigated time point.

Quantitative in vivo analyses corresponding to the ex vivo data strengthened prominent [^{44}Sc]Sc-DOTA-c(RGD)₂ uptake in the tumourous lesions, with %ID/g values of 3.93 ± 1.19 , 3.07 ± 1.17 , and 3.00 ± 1.25 measured 0.5, 2, and 4 h after the injection, respectively. Similar to the PET data, insignificant ex vivo non-target activity was detected. Receptor-blocking studies showed the reduction of the radiotracer uptake of the tumours both in vivo and ex vivo. However, a (cRGD)₂-derived decrease in the tracer concentration was recorded ex vivo in the background organs/tissues, which could be attributed to their physiological $\alpha_v\beta_3$ expression.

Assessing the adhering affinities of cRGD, (cRGD)₂, and DOTA-(cRGD)₂, Hernandez et al. noted that the administration of the investigated peptides induced the concentration-dependent disposition of ^{125}I -echistatin. Although a binding competence 10 times stronger was depicted in the case of (cRGD)₂ relative to its monomeric counterpart, DOTA complexation exerted no meaningful effect on the peptide-targeting affinity of (cRGD)₂. Based on current literature data, Hernandez et al. were the first to propose a peptide-based PET radiopharmaceutical labelled with cyclotron-derived ^{44}Sc . Therefore, they managed

to strengthen the suitability of ^{44}Sc for PET investigations in addition to the already-established radiometals. A summary of their study can be seen in Table 1.

In another study, Domnanich et al. performed an *in vitro* and *in vivo* comparison of DOTA- and NODAGA-conjugated cyclic RGD tripeptide radiolabelled with both ^{44}Sc and ^{68}Ga ($[^{44}\text{Sc}]\text{Sc}/[^{68}\text{Ga}]\text{Ga}$ -DOTA/NODAGA-RGD) (as seen in Table 1) [76]. In this study they also assessed ^{68}Ga - and ^{44}Sc -labelled somatostatin analogue NOC ([Tyr3,1-NaI3]octreotide) complexed with the same chelators ($[^{44}\text{Sc}]\text{Sc}/[^{68}\text{Ga}]\text{Ga}$ -DOTA/NODAGA-NOC). Besides *in vitro* stability examinations, biodistribution and *in vivo* PET-/CT-imaging studies of female athymic nude (CD-1 nude) mice bearing U87MG (human glioblastoma) and AR42J (rat exocrine pancreatic tumour) tumours were conducted. DOTA chelator-derivatized peptides (both RGD and NOC) labelled with either ^{44}Sc or ^{68}Ga showed high *in vitro* stability. Although ^{68}Ga -labelled NODAGA-RGD and NODAGA-NOC were stable during the examination time, NODAGA-conjugated peptides radiolabelled with ^{44}Sc did not present such results. The *in vitro* stability was evaluated in the presence of Fe^{3+} and Cu^{2+} , as well. The instability of $[^{68}\text{Ga}]\text{Ga}$ -DOTA-RGD and $[^{68}\text{Ga}]\text{Ga}$ -DOTA-NOC was registered upon Cu^{2+} administration, whereas ^{44}Sc -labelled molecules coordinated with NODAGA were less stable in the case of the addition of both metal cations. The ^{44}Sc -labelled RGD peptides conjugated with either DOTA or NODAGA showed an identical tumour-distribution profile ($4.88 \pm 0.67\%$ IA/g and $4.50 \pm 0.77\%$ IA/g for $[^{44}\text{Sc}]\text{Sc}$ -DOTA-RGD and $[^{44}\text{Sc}]\text{Sc}$ -NODAGAD-RGD, respectively, at 0.5 h post injection). Intriguingly, the hepatic uptake of $[^{44}\text{Sc}]\text{Sc}$ -DOTA-RGD was more elevated in comparison to the accumulation of $[^{44}\text{Sc}]\text{Sc}$ -NODAGAD-RGD 0.5 h after the tracer injections; however, at later time points similar liver activities were measured. As for other selected organs and tissues, Domnanich et al. experienced the same radiopharmaceutical accretion. The biodistribution profile of the ^{44}Sc -labelled and ^{68}Ga -labelled compounds was compared, as well. The liver showed increased uptake of the ^{68}Ga -labelled DOTA-chelated peptides relative to the ^{44}Sc -appended DOTA matches. This finding was in accordance with the *in vivo* PET data. Regarding other organs, the uptake of the ^{68}Ga and ^{44}Sc peptides was mostly identical. Since the ^{44}Sc -appended molecules complexed with NODAGA demonstrated a largely identical tracer-accumulation pattern compared to the DOTA-chelated ones, NODAGA seems to be an attractive alternative chelator to more established DOTA for the development of ^{44}Sc -labelled PET radiotracers [76].

In a study by Nagy et al., the applicability of mesocyclic chelating agent AAZTA (1,4-bis(carboxymethyl)-6-[bis(carboxymethyl)]amino-6-methylperhydro-1,4-diazepine) for conjugation with ^{44}Sc -labelled PET radiometalated peptides was ratified [77]. The outstanding complex formation between Sc^{III} and AAZTA laid the basis for the proposal of ^{44}Sc -labelled PET-imaging probes chelated by AAZTA. Tumour-naïve healthy control and 4T1 tumour-bearing BALB/c mice were used for the evaluation of the *in vivo* biodistribution of $^{44}\text{Sc}^{3+}$, $^{44}\text{Sc}(\text{AAZTA})^-$, and $^{44}\text{Sc}(\text{CNAAZTA-c(RGDfK)})$ (c(RGDfK): cyclo(-Arg-Gly-Asp-d-Phe-Lys)). The choice of using 4T1 tumours for their experiments was reinforced by the integrin $\alpha_v\beta_3$ overexpression of breast cancers [93]. Positron emission tomography/magnetic resonance imaging (PET/MRI) examinations were performed 30 and 90 min post administration of the free $^{44}\text{Sc}^{3+}$, $^{44}\text{Sc}(\text{AAZTA})^-$ complex, and ^{44}Sc -labelled CNAAZTA-conjugate. Discrete hepatic, pulmonary, and lienal uptake of $^{44}\text{Sc}^{3+}$ was registered on the PET scans of the control group 90 min post injection. In contrast, $^{44}\text{Sc}(\text{AAZTA})^-$ showed no accretion in either the thoracic or the abdominal organs. Investigating the distribution pattern of $^{44}\text{Sc}(\text{CNAAZTA-c(RGDfK)})$, Nagy et al. revealed physiological accumulation in the liver, intestines, and urinary tract of the control BALB/c study mice. Based on the enhanced 4T1 tumour-tracer uptake, the tumour-homing capability of this newly produced $\alpha_v\beta_3$ integrin-affine, ^{44}Sc -labelled, AAZTA-conjugated imaging probe was confirmed. Comparing the radioactivity of the neoplasms with that of the non-target tissues and organs, a radiopharmaceutical concentration 25 times more elevated was encountered in the subcutaneously (*sc.*) growing 4T1 tumours than in the background tissues. Consequently, imaging with $^{44}\text{Sc}(\text{CNAAZTA-c(RGDfK)})$ ensured high T/M ratios, which enable precise differentiation

between the neoplastic alterations and the surrounding healthy tissues. It can be concluded that the application of a chelator other than the one generally used (e.g., DOTA) has no influence on the imaging properties of ^{44}Sc . Furthermore, accurate lesion detection and anatomical localization provided by the appropriate T/M ratios are of crucial significance in terms of PET-image reporting. These findings also support the feasibility of ^{44}Sc -labelled PET probes in tumour diagnostics. The details of their study are presented in Table 1. In a recent study by Ghiani et al., the potential of an AAZTA-chelated PSMA inhibitor (B28110) radiolabelled with ^{44}Sc (^{44}Sc]Sc-B28110) was confirmed for the PET imaging of prostate cancer [94]. For the accomplishment of their study, LNCaP tumour-bearing mice were generated by the sc. transplantation of 5×10^6 PSMA-positive LNCaP (prostate cancer derived from a metastatic lymph-node lesion of a human with prostate cancer) tumour cells into the right-shoulder and the right-thigh region of CB17 SCID male mice. Among others, they investigated the in vivo and ex vivo biodistribution pattern and the tumour-targeting capability of ^{44}Sc - and ^{68}Ga -labelled B28110 (^{44}Sc]Sc-B28110 and ^{68}Ga]Ga-B28110) by performing dynamic (0–90 min) and 20 min-long static (150 min post tracer injection) in vivo PET/MRI examinations in male CB17 SCID mice bearing PSMA-positive LNCaP tumours. Furthermore, the diagnostic feasibility of these novel AAZTA-based imaging probes was compared with that of the DOTA analogue PSMA-617, which contains the same binding sequence. Analysing the PET/MRI scans, increased radiotracer accumulation was registered in the tumorous regions 20 min after the tracer administration. Based on the time-activity curves, ^{44}Sc]Sc-B28110 accumulation was statistically more enhanced in the LNCaP tumours in comparison to the other assessed tracers regarding all time points; however, the tumorous lesions could be clearly detected with the use of all three probes (^{44}Sc]Sc-B28110, ^{68}Ga]Ga-B28110, and ^{44}Sc]Sc-PSMA-617). Based on the ex vivo biodistribution data three hours post tracer application, ^{44}Sc]Sc-B28110 and ^{68}Ga]Ga-B28110 showed the highest concentration in the LNCaP tumours, although no remarkable difference was noted between the accumulation of these two compounds. The ex vivo results also revealed an uptake two times higher of the labelled B28110 derivatives relative to that of the ^{44}Sc]Sc-PSMA-617. Therefore, the findings of Ghiani et al. also strengthened the suitability of AAZTA for the conjugation of ^{44}Sc PET probes in diagnostic settings [94].

3. Bombesin- and Gastrin-Releasing Peptide Receptor (GRPR)

G-protein-coupled gastrin-releasing peptide receptors (GRPR) can be encountered in a diverse array of malignancies, including prostate, breast, colon, pancreatic, and pulmonary tumours [95–102]. Beyond cancer cells, tumour vessels show GRPR expression [103]. Gastrin-releasing peptide (GRP) and GRP analogues exert specific binding potential to GRPR in mammals [104–106]. Bombesin (BBN), which shares functional and structural similarities with mammalian GRP, also has high affinity towards GRPR [95,104]. Previous in vitro and in vivo studies have confirmed that both BBN and GRP possess angiogenic properties [107–109]. Besides modulating the morphology of neoplastic cells, tumour differentiation, and tumour proliferation, activated GRPR catalyses the overexpression of proangiogenic genes [110,111]. BBN-triggered GRPR induces PI3 downstream signalling pathways, including the phosphorylation of angiogenesis-related Akt (protein kinase B) [112–114]. Moreover, the suppression of the BBN/GRPR axis leads to the inhibition of tumour propagation and vascularization [113]. Taking the abovementioned research findings into account, radiolabelled GRPR-targeting BBN or its analogues serve as valuable vectors in receptor-positive lesion detection.

Aminobenzoyl-bombesin analogue (4-aminobenzoyl-Q-W-A-V-G-H-L-M-NH₂, AMBA) is regarded as a highly valuable imaging agent in the nuclear medical diagnostics of GRPR-upregulated tumours [115]. A former preclinical study proved the GRPR-binding ability of ^{18}F - and ^{64}Cu -labelled AMBA derivatives [116]. Furthermore, the targeting potential of DOTA-conjugated AMBA labelled with ^{68}Ga or ^{177}Lu was also reported at the preclinical level [115,117].

Investigating the GRPR selectivity of [⁴⁴Sc]Sc-NODAGA-AMBA, Kálmán-Szabó et al. performed in vitro receptor binding and in vivo examinations using a GRPRpos. PCa PC-3 (prostate cancer) xenograft (displayed in Table 1) [75]. The application of PC-3 cell lines was suitable for these studies, as previous research had confirmed their GRPR positivity [111,118]. The imaging characteristics of [⁴⁴Sc]Sc-NODAGA-AMBA were also compared with the ⁶⁸Ga-labelled match ([⁶⁸Ga]Ga-NODAGA-AMBA). In addition, the pharmacokinetic profile of [⁴⁴Sc]Sc-NODAGA-AMBA and its in vivo and in vitro stability were determined. Based on the in vitro serum-stability measurements, the RCP of the ⁴⁴Sc-appended compound was over 98% at both the 15 and 90 min time points, whereas the RCP of the ⁶⁸Ga-tagged AMBA derivative showed a gradual decrease from 92% to 85% between 15 and 90 min. To authenticate the receptor-binding affinity of [⁴⁴Sc]Sc-NODAGA-AMBA and [⁶⁸Ga]Ga-NODAGA-AMBA, in vitro cellular-uptake studies were executed by applying GRPR-overexpressing human PCa PC-3 and receptor-negative human immortal keratinocyte HaCaT cell lines. Followed by a 60 or 120 min-long incubation with 0.37 MBq of [⁴⁴Sc]Sc-NODAGA-AMBA or [⁶⁸Ga]Ga-NODAGA-AMBA, the samples were measured for radioactivity in a gamma counter to provide uptake values in %ID/million cell units. Receptor-upregulated PC-3 cells presented notably higher (25 times) accumulation of both [⁴⁴Sc]Sc-NODAGA-AMBA and [⁶⁸Ga]Ga-NODAGA-AMBA than receptor-negative HaCaT cells ($p < 0.01$). Although from statistical point of view no considerable difference was encountered between the accumulation of the ⁴⁴Sc-appended and the ⁶⁸Ga-labelled radiotracers in the tumour cells, they expressed relatively more elevated [⁴⁴Sc]Sc-NODAGA-AMBA uptake compared to [⁶⁸Ga]Ga-NODAGA-AMBA ($p < 0.05$). Furthermore, in vitro blocking investigations performed with 200 nM BBN as blocking agent revealed that the tracer uptake of the PC-3 cells was remarkably diminished, whereas the radioactivity of the control cells remained unchanged. Analytical radio-HPLC-based in vivo serum-stability calculations conducted in healthy mice proved outstanding metabolic stability in the case of both probes. According to the pharmacokinetic investigations—similar to [⁶⁸Ga]Ga-NODAGA-AMBA—[⁴⁴Sc]Sc-NODAGA-AMBA possessed a circulatory half-life shorter than 30 min.

In a bid to conduct in vivo and ex vivo measurements, 12-week-old, severe combined immunodeficient (SCID) CB17 mice bearing PC-3 prostate cancer in their left-shoulder area and healthy control mice were examined. For the assessment of the biodistribution pattern of the probes, 60 and 120 min post injections of 11.3 ± 1.4 MBq of [⁴⁴Sc]Sc-NODAGA-AMBA or [⁶⁸Ga]Ga-NODAGA-AMBA static PET acquisition were conducted with the application of a miniPET device (University of Debrecen, Faculty of Medicine, Department of Medical Imaging, Division of Nuclear Medicine and Translational Imaging). Standardized uptake values (SUV) and T/M ratios were registered to quantify the radiopharmaceutical uptake. Both qualitative analyses and quantitative SUV data confirmed the GRPR-targeting adequacy of the investigated radiolabelled AMBA derivatives. Although 60 min post administration of [⁴⁴Sc]Sc-NODAGA-AMBA higher SUV_{mean} (0.90 ± 0.17), SUV_{max} (1.54 ± 0.18), T/M SUV_{mean} (6.16 ± 1.24), and T/M SUV_{max} (6.71 ± 1.08) values of the sc. growing PC-3 tumours were registered compared to the ⁶⁸Ga-labelled counterpart, this was not statistically significant ($p \leq 0.05$). Moreover, 120 min after the injection of the radiotracers, decreased non-target activity was observed, which led to excellent T/M ratios.

Ex vivo biodistribution studies of both the healthy control and the tumour-bearing mice were accomplished 30, 60, 120, and 180 min after the administration of 11.3 ± 1.4 MBq of [⁴⁴Sc]Sc-NODAGA-AMBA or [⁶⁸Ga]Ga-NODAGA-AMBA. The radioactivity of the explanted tissues and organs was registered with a calibrated gamma counter, and the counts-per-minute (CPM) values of all samples were converted to the percentage of administered dose per gram of tissue. The radiotracer concentration was presented as %ID/g. The biodistribution pattern of the control small animals displayed lower accumulation of [⁴⁴Sc]Sc-NODAGA-AMBA relative to [⁶⁸Ga]Ga-NODAGA-AMBA; however, this difference was not statistically significant ($p < 0.05$). After analysing the tracer uptake of the organs separately, the blood, liver, spleen, small and large intestines, stomach, heart, and lungs

were depicted with moderate radioactivity, whereas the kidneys, urine, adrenal glands, and pancreas demonstrated significant tracer accretion. The outstanding urinary activity could have been due to the renal method of elimination or the physiological presence of GRPR in the urogenital smooth muscle [119]. The natural appearance of GRPR in the pancreas and in the adrenal glands underlies the remarkable radiotracer uptake of these organs [105,120]. Discrete receptor expression of the neuroendocrine gastrointestinal cells and the pulmonary existence of the GRPR gene may explain tracer accumulation in the lungs and in the intestines [121,122]. In line with the *in vivo* findings, the [⁴⁴Sc]Sc-NODAGA-AMBA uptake of the PC-3 tumours was more prominent in comparison to the ⁶⁸Ga-labelled derivative.

Receptor-suppressing *in vivo* and *ex vivo* studies were carried out with the injection of 15 mg/kg of BBN into the tumorous study mice 30 min before radiotracer application to further ratify the GRPR selectivity of the labelled BBN analogues. Correspondingly to the *ex vivo* blocking figures, both qualitative and quantitative *in vivo* analyses revealed considerably mitigated tracer uptakes in the PC-3 tumours 60 and 120 min post injection.

Given the GRPR selectivity of [⁴⁴Sc]Sc-NODAGA-AMBA established by Kálmán-Szabó et al., along with the better imaging characteristics of ⁴⁴Sc over ⁶⁸Ga, ⁴⁴Sc-labelled BBN-based radiotracers, will hopefully be embraced in the diagnostic armamentarium of GRPRpos. tumours.

Another investigation, executed by Koumarianou et al., focused on the comparison of ⁴⁴Sc- and ⁶⁸Ga-labelled BBN analogues in *in vitro* and *in vivo* biological medium [33]. In a bid to evaluate the potential impact of ⁴⁴Sc on the binding ability of BBN analogue to GRPR, GRPR-affine DOTA-conjugated BBN analogue was labelled with ⁶⁸Ga and ⁴⁴Sc, and the *in vitro* receptor-adhering capacity, the *ex vivo* organ distribution, and the *in vivo* behaviour of both ⁴⁴Sc-DOTA-BN[2-14]NH₂ and ⁶⁸Ga-DOTA-BN[2-14]NH₂ were assessed. Table 1 shows the major points of their research.

DOTA-BN[2-14]NH₂ complexed with ^{nat}Ga and ^{nat}Sc were used as non-radioactive derivatives to study *in vitro* GRPR-binding competence in competition with radiolabelled BBN analogue [¹²⁵I-Tyr⁴]-BN in the human androgen-independent prostate-cancer PC-3 cell line. Thereafter, organ distribution was investigated in healthy male Sprague-Dawley rats one and two hours after the intravenous (*iv.*) administration of 11 and 3 MBq ⁶⁸Ga-DOTA-BN[2-14]NH₂ and ⁴⁴Sc-DOTA-BN[2-14]NH₂, respectively, via the jugular vein. As part of the biodistribution studies, blocking experiments were also performed with the *iv.* application of native BBN (100 µg/100 µL) 15 min before the radiotracer injection. The organ-distribution pattern of the control cohort—solely receiving the radiolabelled analogue—and that of the blocked group was compared. Androgen-independent Dunning R-3327-AT-1 prostate-cancer tumour-bearing small animals were generated by the subcutaneous (*sc.*) transplantation of GRPR-overexpressing R-3327-AT-1 cells (≈0.4 mL, 10⁴ cells/µL) into the dorsal aspect of the hind foot of male Copenhagen rats [33,123]. Dynamic microPET acquisition was executed approximately 10–14 days post tumour induction by applying 30–50 MBq of either the ⁶⁸Ga- or the ⁴⁴Sc-appended imaging probes. ^{nat}Ga-DOTA-BN[2-14]NH₂ showed higher specificity towards GRPR receptors than the ^{nat}Sc-complexed counterpart. The pancreas was presented with considerable uptake using both labelled compounds with ID/g values of 0.64 ± 0.00% and 0.58 ± 0.05% for ⁶⁸Ga-DOTA-BN[2-14]NH₂ 1 and 2 h post injection, respectively, whereas the subsequent data were obtained in the case of the ⁴⁴Sc-labelled probe: 2.67 ± 0.53% ID/g and 1.51 ± 1.19% ID/g one and two hours after tracer administration, respectively. The physiological pancreatic GRPR expression could explain these results. Upon visual assessment of the *in vivo* PET images, the peripheral tumour areas demonstrated more enhanced tracer uptake compared to the central neoplastic regions. The heterogeneity of the receptor expression within the tumour and the unevenness regarding the radiopharmaceutical binding ability of GRPR could underpin the difference between the tracer accretion of the external and inner tumour regions. Followed by prompt radiotracer uptake post injection, Koumarinaou et al. noted a gradual decline in the accumulation kinetics of the ⁶⁸Ga-labelled compound throughout the entire examination period, whereas they observed a stable albeit lower tracer uptake in the

case of the ^{44}Sc -appended match. Of note, the relative tumour radioactivity-based kinetics (normalized to the testis as a reference tissue) did not reveal any meaningful differences between the two tracers. Overall, the GRPR selectivity of ^{68}Ga and ^{44}Sc differed. However, given the similar distribution pattern, uptake, and excretion times of both the ^{68}Ga - and the ^{44}Sc -labelled radiopharmaceuticals, as well as their comparable accumulation in neoplastic tissues, these radiometals seemed equally effective in the detection of GRPRpos. tumours [33].

4. Hypoxia-Associated 2-Nitroimidazole (NI) Derivatives

Beyond the above-mentioned radiopharmaceuticals, hypoxia-associated PET tracers are also embraced in tumour diagnostics [124–126]. Since cancer-related neoangiogenesis, induced by oxygen insufficiency, leads to morphologically and functionally impaired blood-vessel development, which directly affects the efficiency of anti-tumour treatment, the early identification of hypoxic tumorous regions is of paramount importance [127–129]. In this respect, hypoxia-directed imaging probes could be potential weapons in the timely diagnostic assessment of tumour-related hypoxia and the achievement of therapeutic successes.

Given the fact that hypoxia-associated 2-nitroimidazole (NI) derivatives are intracellularly trapped under hypoxic conditions while they are reoxidised and excreted from normoxic cells, by applying NI-based imaging probes, healthy and hypoxic tumorous cells could be definitively differentiated from each other [130]. Therefore, NI compounds labelled with radioisotopes seem to be promising indicators of tumour-associated hypoxia. Previous successes were attained in clinical trials by applying ^{18}F -labelled NI-derivatives such as [^{18}F]F-fluoromisonidazole ([^{18}F]F-FMISO) and [^{18}F]F-fluoroazomycin arabinoside ([^{18}F]F-FAZA) in hypoxia imaging [131,132]. Barthel et al., Yang et al., and Ziemer et al. proposed [^{18}F]F-fluoroetanidazole ([^{18}F]F-FETA), [^{18}F]F-fluoroerythronitroimidazole ([^{18}F]F-FETNIM), and [^{18}F]F-[2-(2-nitro-1[H]-imidazol-1-yl)-N-(2,2,3,3,3-pentafluoropropyl)-acetamide] ([^{18}F]F-EF5), respectively, for the non-invasive detection of cancer-related hypoxia [124–126]. However, the low T/M ratios generated by the prolonged elimination of these lipophilic tracers may hamper their widespread application in diagnostic fields. In 2011, Hoigebazar et al. verified the feasibility of ^{68}Ga -labelled DO3AM-NI in hypoxia PET imaging [133].

Later in 2022, Szücs et al. published the synthesis of ^{44}Sc -appended hypoxia-specific DO3AM-NI (^{44}Sc]Sc-DO3AM-NI) and its comparison to the ^{68}Ga -labelled diagnostic match [78]. To study the *in vivo* and the *ex vivo* biodistribution of the ^{44}Sc and ^{68}Ga hypoxia PET probes, healthy and CB17 SCID adult male mice bearing KB (human epidermal carcinoma) tumours in their left-shoulder area were applied (presented in Table 1). *In vivo* PET/MRI studies were conducted 13 ± 1 days post implantation of 5×10^6 KB tumour cells at an average tumour bulk of 110 mm^3 . Both the control and the tumorous study mice were *iv.* administered with $8.42 \pm 0.38 \text{ MBq}$ of [^{44}Sc]Sc-DO3AM-NI and [^{68}Ga]Ga-DO3AM-NI. Then, whole-body T1-weighted MRI and 20 min-long static whole-body PET acquisition was performed 90 and 240 min post tracer application. SUV and T/M ratios (ratios of tumour to skeletal muscles of the right-shoulder region) were defined as quantitative PET parameters. Ninety minutes and 4 h (240 min) post injection, organ-tissue specimens were harvested, weighed wet, and measured for radiopharmaceutical uptake by applying a gamma counter to obtain *ex vivo* data. Values were provided as mean %ID/g \pm SD. Szücs et al. managed to label the NI derivative DO3AM-NI with ^{44}Sc with a high-labelling yield and RCP. Except for the kidneys and the urinary bladder, the organs of the abdomen and thorax displayed moderate tracer accretion upon visual assessment of the PET scans. The high uptake of both probes in the kidney underpinned its important role in radiopharmaceutical elimination. Intriguingly, enhanced hepatic [^{68}Ga]Ga-DO3AM-NI concentration was visually depicted 90 min post injection. The ^{44}Sc -labelled NI-based counterpart accumulated rapidly in the sc. developing KB tumours and produced satisfactory images at 90 min and 240 min post tracer injection (SUV_{mean}: 1.46 ± 0.32 , 0.67 ± 0.03 at 90 and 240 min time points, respectively; SUV_{max}: 2.35 ± 0.47 and

1.55 ± 0.28 at 90 and 240 min time points, respectively). Although the quantitative tumour uptakes of [⁴⁴Sc]Sc-DO3AM-NI and [⁶⁸Ga]Ga-DO3AM-NI were comparable, the liver, spleen, kidneys, intestines, lung, heart, and brain were depicted with higher [⁶⁸Ga]Ga-DO3AM-NI uptake compared to the ⁴⁴Sc counterpart 90 and 240 min post injection. More elevated accretion of the ⁶⁸Ga-linked tracer in the non-target organs led to T/M ratios 10–15 times lower relative to the ⁴⁴Sc-labelled derivative. In the case of [⁶⁸Ga]Ga-DO3AM-NI, T/M SUV_{mean} and T/M SUV_{max} values of 85.66 ± 6.06 and 41.72 ± 13.61 were experienced, respectively, whereas for [⁴⁴Sc]Sc-DO3AM-NI the following parameters were defined: T/M SUV_{mean}: 182.67 ± 23.50 and T/M SUV_{max}: 129.68 ± 26.11 4 h after the injection. Hence, outstanding lesion identification, which could be derived from the suitable T/M ratios of the ⁴⁴Sc-labelled derivative, warrants a place for ⁴⁴Sc in the targeted PET imaging of hypoxia-related tumour diagnostics. Unlike these findings, previous studies dealing with ¹⁸F, iodine-131 (¹³¹I), technetium-99m (^{99m}Tc), and ⁶⁴Cu-appended NI imaging probes reported substantial tracer accumulation in the abdominal organs, mainly in the intestines, along with hepatic metabolization, which could lead to difficulties regarding the detection of abdominal malignancies [134–137].

In line with the *in vivo* findings, the *ex vivo* figures revealed that the KB tumour uptake of the two investigated probes did not differ significantly between the two assessed time points; however, the accumulation of the ⁴⁴Sc pendant was more prominent in comparison to the ⁶⁸Ga-labelled compound both 90 and 240 min post injection. In agreement with the *in vivo* results, considerably higher T/M ratios were registered in connection with [⁴⁴Sc]Sc-DO3AM-NI than [⁶⁸Ga]Ga-DO3AM-NI ($p \leq 0.01$). In addition, the *ex vivo* organ-distribution pattern also confirmed notably lower [⁴⁴Sc]Sc-DO3AM-NI uptake in the evaluated organs compared to the ⁶⁸Ga-labelled sister compound ($p \leq 0.01$). The biodistribution results of Hoigebazar et al. and Seelam et al. regarding NI compounds labelled with ⁶⁸Ga were in accordance with those of Szücs et al. [138,139]. In addition to the urinary method of excretion, they registered discrete radioactivity in the abdominal and thoracic organs [138,139]. As for the visualization of the PET scans, due to prompt urinary clearance and favourable T/M ratios, [⁴⁴Sc]Sc-DO3AM-NI seemed to be superior to the ^{99m}Tc-, ⁶⁴Cu-, ¹⁸F-, ¹³¹I-, and ⁶⁸Ga-linked derivatives. Based on the exceptional tumour-homing capability, appropriate contrast and favourable quantitative parameters of the ⁴⁴Sc-appended molecular agent [⁴⁴Sc]Sc-DO3AM-NI could be a highly valuable hypoxia-targeting PET probe in the diagnostic algorithm of tumour identification.

5. Vascular Endothelial Growth Factor Receptor (VEGFR)

VEGFs, including VEGF-A, -B, -C, -D, and -E, and placenta growth factor (PlGF) also have a pivotal role in blood-vessel formation [140,141]. The interplay between VEGF-A, VEGFR-2, and neuropilin-1 (NRP-1) co-receptor constitutes a crucial step in angiogenesis [142]. In addition, NRP-1 is presented in different cancer-cell lines and primary malignancies, including lung, renal, and breast cancer, as well as glioblastoma multiforme [143–146]. Consequently, biomolecules designed to target VEGF, its receptors, or NRP-1 have gained increasing attention in oncological research [147].

Although no previous *in vivo* experiments that investigated ⁴⁴Sc-labelled VEGF-VEGFR-NRP-1-directed radiopharmaceuticals have been published so far, Masłowska et al. examined the potential diagnostic and therapeutic feasibility of such molecules under *in vitro* circumstances [79].

With the aim of inhibiting the formation of the vascular endothelial growth factor/neuropilin-1 co-receptor complex VEGF-A₁₆₅/NRP-1, Masłowska et al. developed NRP-1-targeting radiotracers [79]. In their study, three NRP-1-affine molecules were labelled with ⁴⁴Sc: Ala-Thr-Trp-Leu-Pro-Pro-Arg (A7R) heptapeptide, branched peptidomimetic Lys(hArg)-Dab-Pro-Arg (K4R), and the retro-inverso isomer of A7R (dArg-dPro-dPro-dLeu-dTrp-dThr-dAla) named ^DR7A. For verification of their NRP-1 selectivity, a competitive NRP-1-binding inhibition assay was performed using enzyme-linked immunosorbent assay (ELISA). After the addition of recombinant human NRP-1 (100 µL; 200 ng/well) to a 96-well plate, 50 µL of

the solution of the cold reference molecules of the assessed tracers and 50 μL (400 ng/mL) of human biotinylated VEGF- A_{165} ((bt)-VEGF- A_{165}) were administered. Wells treated with (bt)-VEGF- A_{165} were the positive controls, whereas wells without NRP-1 were the negative controls. The IC_{50} values of the following cold biomolecules—Sc-DOTA-Ahx-A7R, Lys(DOTA-Sc)-A7R, and Lys(hArg)-Dab(Ahx-DOTA-Sc)-Pro-Arg—indicated high affinity towards NRP-1, meaning that their radiolabelled counterparts (^{44}Sc]Sc-DOTA-Ahx-A7R, ^{44}Sc]Lys(DOTA-Sc)-A7R, and ^{44}Sc]Sc-DOTA-Ahx-K4R) could be effectively used to prevent the development of VEGF- A_{165} /NRP-1 complex. Hence, they could widen the existing scale of the diagnostic and therapeutic probes applied in cancer-related angiogenesis. In contrast, retro-inverso peptide $^{\text{D}}$ R7A-based compounds exerted low NRP-1 specificity. However, due to the inadequate human-serum stability of the evaluated agents, future studies are required for the optimization of their usage for therapeutic purposes.

6. Aminopeptidase N (APN/CD13)

Out of the neo/angiogenesis-related molecules, another intensively investigated one is the aminopeptidase N receptor (APN/CD13) [148]. The association between Zn^{2+} -dependent membrane-bound ANP/CD13 and cell differentiation, motility, proliferation, cell death, and angiogenic processes is well-established [149]. According to existing literature, among others, melanoma-, prostate-, pulmonary-, breast-, and ovarian-cancer cells express APN/CD13 [148, 150–152]. Peptides with the asparagine–glycine–arginine sequence (tripeptide NGR) show selective APN/CD13pos. tumour-targeting capability [153]. Considering that APN/CD13 positivity is directly proportional to tumour aggressiveness, NGR-motif-based imaging probes could be promising in the identification of APN/CD13-overexpressing neoplasms. Beyond diagnostic applications, NGR-containing molecules also act as chemotherapeutic drug carriers, thus serving as a useful means of directed anti-cancer treatment choices [154–156]. Previous studies by Máté et al., Kis et al., and Gyuricza et al. have confirmed the diagnostic potential of NGR agents radiolabelled with ^{68}Ga in the detection of tumours with APN/CD13 up-regulation [157–159]. Other studies conducted by Li et al., Ma et al., and Vats et al. applied ^{64}Cu , rhenium-188 (^{188}Re), and ^{177}Lu , respectively, for labelling purposes of NGR radiopharmaceuticals [160–162]. Although no former findings regarding ^{44}Sc -labelled NGR-based radiotracers are available so far, ^{44}Sc could be a potential radionuclide for the labelling of APN/CD13-targeting imaging vectors.

7. Conclusions

The *in vivo* tumour-targeting capability of ^{44}Sc -labelled, angiogenesis-targeting imaging probes, along with the favourable physicochemical properties of the radiometal, capitalize on the relevance of this isotope for the development of highly specific PET radiotracers. Their transition into clinical routine will inevitably herald a new era in personalized cancer diagnostics. Furthermore, the non-invasive assessment of angiogenesis-/neo-angiogenesis-related molecules is of outstanding importance to identifying patients who may benefit from targeted antiangiogenic therapy. Together with its therapeutic surrogate, the $^{44}\text{Sc}/^{47}\text{Sc}$ isotopic pair could be effectively employed in dosimetry estimations, cancer treatment, and therapeutic follow-up.

However, the future progression of ^{44}Sc -labelled molecular vectors from preclinical level to human application could be hampered by some constraints regarding the usage of ^{44}Sc . First, the limited accessibility of the radiometal is a meaningful hurdle to its centralized distribution. In addition, the high-energy concomitant gamma rays (1157 keV) of ^{44}Sc could lead to reduced image quality; therefore, future studies to optimize PET-imaging parameters are required [32]. Furthermore, ^{43}Sc lacking in accompanying gamma co-emission may serve as a valuable substitute for ^{44}Sc in imaging settings [46]. Global steps should be taken to overcome these drawbacks, with the ultimate goal of exploiting both the diagnostic and therapeutic value of ^{44}Sc .

Author Contributions: Z.K.: conceptualization, writing—original draft; G.T.: conceptualization, writing—review and editing, supervision. All authors have read and agreed to the published version of the manuscript.

Funding: This research received no external funding.

Institutional Review Board Statement: Not applicable.

Informed Consent Statement: Not applicable.

Data Availability Statement: The datasets used and/or analysed during the current study are available from the corresponding author upon reasonable request.

Conflicts of Interest: The authors declare no conflict of interest.

References

1. Folkman, J. Role of angiogenesis in tumor growth and metastasis. *Semin. Oncol.* **2002**, *29*, 15–18. [[CrossRef](#)] [[PubMed](#)]
2. Jiménez, B. Mechanistic insights on the inhibition of tumor angiogenesis. *J. Mol. Med.* **2001**, *78*, 663–672. [[CrossRef](#)] [[PubMed](#)]
3. Hanahan, D.; Folkman, J. Patterns and Emerging Mechanisms of the Angiogenic Switch during Tumorigenesis. *Cell* **1996**, *86*, 353–364. [[CrossRef](#)] [[PubMed](#)]
4. Folkman, J. Tumor angiogenesis. In *Cancer Medicine*, 5th ed.; Holland, J.F., Frei, E., III, Bast, R.C., Jr., Eds.; B.C. Decker: Hamilton, ON, Canada, 2000; pp. 132–152.
5. Folkman, J. Angiogenesis. In *Harrison's Principles of Internal Medicine*, 15th ed.; Braunwald, E., Fauci, A.S., Kasper, D.L., Hauser, S.L., Longo, D.L., Jameson, J.L., et al., Eds.; McGraw-Hill: New York, NY, USA, 2001; pp. 517–530.
6. Whitelock, J.M.; Murdoch, A.D.; Iozzo, R.V.; Underwood, P.A. The Degradation of Human Endothelial Cell-derived Perlecan and Release of Bound Basic Fibroblast Growth Factor by Stromelysin, Collagenase, Plasmin, and Heparanases. *J. Biol. Chem.* **1996**, *271*, 10079–10086. [[CrossRef](#)] [[PubMed](#)]
7. Lugano, R.; Ramachandran, M.; Dimberg, A. Tumor angiogenesis: Causes, consequences, challenges and opportunities. *Cell. Mol. Life Sci.* **2020**, *77*, 1745–1770. [[CrossRef](#)]
8. Asabella, A.N.; Altini, C.; Ferrari, C.; Rubini, G.; Di Palo, A. Multimodality Imaging in Tumor Angiogenesis: Present Status and Perspectives. *Int. J. Mol. Sci.* **2017**, *18*, 1864. [[CrossRef](#)]
9. Carmeliet, P.; Jain, R.K. Molecular mechanisms and clinical applications of angiogenesis. *Nature* **2011**, *473*, 298–307. [[CrossRef](#)]
10. Bergsland, E.K. Update on Clinical Trials Targeting Vascular Endothelial Growth Factor in Cancer. *Am. J. Health Pharm.* **2004**, *61*, S12–S20. [[CrossRef](#)]
11. Siemann, D.W.; Chaplin, D.J.; Horsman, M. Vascular-targeting therapies for treatment of malignant disease. *Cancer* **2004**, *100*, 2491–2499. [[CrossRef](#)]
12. Stacy, M.R.; Maxfield, M.W.; Sinusas, A.J. Targeted molecular imaging of angiogenesis in PET and SPECT: A review. *Yale J. Biol. Med.* **2012**, *85*, 75–86.
13. Huclier-Markai, S.; Alliot, C.; Kerdjoudj, R.; Mougin-Degraef, M.; Chouin, N.; Haddad, F. Promising Scandium Radionuclides for Nuclear Medicine: A Review on the Production and Chemistry up to In Vivo Proofs of Concept. *Cancer Biotherapy Radiopharm.* **2018**, *33*, 316–329. [[CrossRef](#)] [[PubMed](#)]
14. Vaughn, B.A.; Koller, A.J.; Chen, Z.; Ahn, S.H.; Loveless, C.S.; Cingoranelli, S.J.; Yang, Y.; Cirri, A.; Johnson, C.J.; Lapi, S.E.; et al. Homologous Structural, Chemical, and Biological Behavior of Sc and Lu Complexes of the Picaga Bifunctional Chelator: Toward Development of Matched Theranostic Pairs for Radiopharmaceutical Applications. *Bioconjugate Chem.* **2021**, *32*, 1232–1241. [[CrossRef](#)] [[PubMed](#)]
15. Snow, M.S.; Foley, A.; Ward, J.L.; Kinlaw, M.T.; Stoner, J.; Carney, K.P. High purity ^{47}Sc production using high-energy photons and natural vanadium targets. *Appl. Radiat. Isot.* **2021**, *178*, 109934. [[CrossRef](#)] [[PubMed](#)]
16. Türler, A. Matched Pair Theranostics. *Chimia* **2019**, *73*, 947–949. [[CrossRef](#)]
17. Hernandez, R.; Valdovinos, H.F.; Yang, Y.; Chakravarty, R.; Hong, H.; Barnhart, T.E.; Cai, W. ^{44}Sc : An Attractive Isotope for Peptide-Based PET Imaging. *Mol. Pharm.* **2014**, *11*, 2954–2961. [[CrossRef](#)]
18. Severin, G.; Engle, J.W.; Valdovinos, H.; Barnhart, T.; Nickles, R. Cyclotron produced ^{44}gSc from natural calcium. *Appl. Radiat. Isot.* **2012**, *70*, 1526–1530. [[CrossRef](#)]
19. Valdovinos, H.; Hernandez, R.; Barnhart, T.; Graves, S.; Cai, W.; Nickles, R. Separation of cyclotron-produced ^{44}Sc from a natural calcium target using a dipentyl pentylphosphonate functionalized extraction resin. *Appl. Radiat. Isot.* **2015**, *95*, 23–29. [[CrossRef](#)]
20. van der Meulen, N.P.; Bunka, M.; Domnanich, K.A.; Müller, C.; Haller, S.; Vermeulen, C.; Türler, A.; Schibli, R. Cyclotron production of ^{44}Sc : From bench to bedside. *Nucl. Med. Biol.* **2015**, *42*, 745–751. [[CrossRef](#)]
21. Norman, E.B.; Browne, E.; Chan, Y.D.; Goldman, I.D.; Larimer, R.-M.; Lesko, K.T.; Nelson, M.; Wietfeldt, F.E.; Zlimer, I. Half-life of ^{44}Ti . *Phys. Rev. C* **1998**, *57*, 2010–2016. [[CrossRef](#)]
22. Roesch, F. Scandium-44: Benefits of a long-lived PET radionuclide available from the $(^{44}\text{Ti})/(^{44}\text{Sc})$ generator system. *Curr. Radiopharm.* **2012**, *5*, 187–201. [[CrossRef](#)]

23. Welch, M.J.; McCarthy, T.J. The potential role of generator-produced radiopharmaceuticals in clinical PET. *J. Nucl. Med.* **2000**, *41*, 315–317. [[PubMed](#)]
24. Filosofov, D.V.; Loktionova, N.S.; Rösch, F. A $^{44}\text{Ti}/^{44}\text{Sc}$ radionuclide generator for potential application of ^{44}Sc -based PET-radiopharmaceuticals. *Radiochim. Acta* **2010**, *98*, 149–156. [[CrossRef](#)]
25. García-Toraño, E.; Peyres, V.; Roteta, M.; Sánchez-Cabezudo, A.; Romero, E.; Ortega, A.M. Standardisation and precise determination of the half-life of ^{44}Sc . *Appl. Radiat. Isot.* **2016**, *109*, 314–318. [[CrossRef](#)] [[PubMed](#)]
26. Mikolajczak, R.; Huclier-Markai, S.; Alliot, C.; Haddad, F.; Szikra, D.; Forgacs, V.; Garnuszek, P. Production of scandium radionuclides for theranostic applications: Towards standardization of quality requirements. *EJNMMI. Radiopharm. Chem.* **2021**, *6*, 19. [[CrossRef](#)] [[PubMed](#)]
27. Sitarz, M.; Cussonneau, J.-P.; Matulewicz, T.; Haddad, F. Radionuclide candidates for $\beta+\gamma$ coincidence PET: An overview. *Appl. Radiat. Isot.* **2020**, *155*, 108898. [[CrossRef](#)]
28. Ferguson, S.; Jans, H.-S.; Wuest, M.; Riauka, T.; Wuest, F. Comparison of scandium-44 g with other PET radionuclides in pre-clinical PET phantom imaging. *EJNMMI Phys.* **2019**, *6*, 23. [[CrossRef](#)]
29. Martiniova, L.; De Palatis, L.; Etchebehere, E.; Ravizzini, G. Gallium-68 in Medical Imaging. *Curr. Radiopharm.* **2016**, *9*, 187–207. [[CrossRef](#)]
30. Rahmim, A.; Zaidi, H. PET versus SPECT: Strengths, limitations and challenges. *Nucl. Med. Commun.* **2008**, *29*, 193–207. [[CrossRef](#)]
31. Rösch, F.; Baum, R.P. Generator-based PET radiopharmaceuticals for molecular imaging of tumours: On the way to THERANOSTICS. *Dalton Trans.* **2011**, *40*, 6104–6111. [[CrossRef](#)]
32. Eppard, E.; de la Fuente, A.; Benešová, M.; Khawar, A.; Bundschuh, R.A.; Gärtner, F.C.; Kreppel, B.; Kopka, K.; Essler, M.; Rösch, F. Clinical Translation and First In-Human Use of [^{44}Sc]Sc-PSMA-617 for PET Imaging of Metastasized Castrate-Resistant Prostate Cancer. *Theranostics* **2017**, *7*, 4359–4369. [[CrossRef](#)]
33. Koumariou, E.; Loktionova, N.; Fellner, M.; Roesch, F.; Thews, O.; Pawlak, D.; Archimandritis, S.; Mikolajczak, R. ^{44}Sc -DOTA-BN[2-14]NH₂ in comparison to ^{68}Ga -DOTA-BN[2-14]NH₂ in pre-clinical investigation. Is ^{44}Sc a potential radionuclide for PET? *Appl. Radiat. Isot.* **2012**, *70*, 2669–2676. [[CrossRef](#)] [[PubMed](#)]
34. Eppard, E. Pre-Therapeutic Dosimetry Employing Scandium-44 for Radiolabeling PSMA-617. In *Prostatectomy*; IntechOpen: London, UK, 2019. [[CrossRef](#)]
35. Kostelnik, T.I.; Orvig, C. Radioactive Main Group and Rare Earth Metals for Imaging and Therapy. *Chem. Rev.* **2019**, *119*, 902–956. [[CrossRef](#)] [[PubMed](#)]
36. Khawar, A.M.; Eppard, E.; Sinnes, J.P.D.; Roesch, F.; Ahmadzadehfar, H.M.; Kürpig, S.; Meisenheimer, M.M.; Gaertner, F.C.; Essler, M.; Bundschuh, R.A. [^{44}Sc]Sc-PSMA-617 Biodistribution and Dosimetry in Patients With Metastatic Castration-Resistant Prostate Carcinoma. *Clin. Nucl. Med.* **2018**, *43*, 323–330. [[CrossRef](#)] [[PubMed](#)]
37. Umbricht, C.A.; Benešová, M.; Schmid, R.M.; Türler, A.; Schibli, R.; van der Meulen, N.P.; Müller, C. ^{44}Sc -PSMA-617 for radiotheragnostics in tandem with ^{177}Lu -PSMA-617—Preclinical investigations in comparison with ^{68}Ga -PSMA-11 and ^{68}Ga -PSMA-617. *EJNMMI Res.* **2017**, *7*, 9. [[CrossRef](#)] [[PubMed](#)]
38. Morgenstern, A.; Apostolidis, C.; Kratochwil, C.; Sathege, M.; Krolicki, L.; Bruchertseifer, F. An Overview of Targeted Alpha Therapy with ^{225}Ac and ^{213}Bi . *Curr. Radiopharm.* **2018**, *11*, 200–208. [[CrossRef](#)] [[PubMed](#)]
39. Deilami-Nezhad, L.; Moghaddam-Banaem, L.; Sadeghi, M. Development of bone seeker radiopharmaceuticals by Scandium-47 and estimation of human absorbed dose. *Appl. Radiat. Isot.* **2017**, *129*, 108–116. [[CrossRef](#)]
40. Majkowska-Pilip, A.; Bilewicz, A. Macrocyclic complexes of scandium radionuclides as precursors for diagnostic and therapeutic radiopharmaceuticals. *J. Inorg. Biochem.* **2011**, *105*, 313–320. [[CrossRef](#)]
41. Viola-Villegas, N.; Doyle, R.P. The coordination chemistry of 1,4,7,10-tetraazacyclododecane- $\text{N},\text{N}',\text{N}'',\text{N}'''$ -tetraacetic acid (H₄DOTA): Structural overview and analyses on structure–stability relationships. *Co-ord. Chem. Rev.* **2009**, *253*, 1906–1925. [[CrossRef](#)]
42. Chakravarty, R.; Goel, S.; Valdovinos, H.F.; Hernandez, R.; Hong, H.; Nickles, R.J.; Cai, W. Matching the Decay Half-Life with the Biological Half-Life: ImmunoPET Imaging with ^{44}Sc -Labeled Cetuximab Fab Fragment. *Bioconjugate Chem.* **2014**, *25*, 2197–2204. [[CrossRef](#)]
43. Nagy, G.; Dénes, N.; Kis, A.; Szabó, J.P.; Berényi, E.; Garai, I.; Bai, P.; Hajdu, I.; Szikra, D.; Trencsényi, G. Preclinical evaluation of melanocortin-1 receptor (MC1-R) specific ^{68}Ga - and ^{44}Sc -labeled DOTA-NAPamide in melanoma imaging. *Eur. J. Pharm. Sci.* **2017**, *106*, 336–344. [[CrossRef](#)]
44. Mausner, L.F.; Joshi, V.; Kolsky, K.L. Evaluation of chelating agents for radioimmunotherapy with scandium-47. *J. Nucl. Med.* **1995**, *36*.
45. Kolsky, K.; Joshi, V.; Mausner, L.; Srivastava, S. Radiochemical purification of no-carrier-added scandium-47 for radioimmunotherapy. *Appl. Radiat. Isot.* **1998**, *49*, 1541–1549. [[CrossRef](#)] [[PubMed](#)]
46. Lima, T.V.M.; Gnesin, S.; Strobel, K.; Pérez, M.D.S.; Roos, J.E.; Müller, C.; van der Meulen, N.P. Fifty Shades of Scandium: Comparative Study of PET Capabilities Using Sc-43 and Sc-44 with Respect to Conventional Clinical Radionuclides. *Diagnostics* **2021**, *11*, 1826. [[CrossRef](#)] [[PubMed](#)]

47. Singh, A.; van der Meulen, N.P.; Grubmüller, B.; Klette, I.; Kulkarni, H.R.; Türler, A.; Schibli, R.; Baum, R.P.; Dash, A.; Chakraborty, S.; et al. First-in-Human PET/CT Imaging of Metastatic Neuroendocrine Neoplasms with Cyclotron-Produced ⁴⁴Sc-DOTATOC: A Proof-of-Concept Study. *Cancer Biotherapy Radiopharm.* **2017**, *32*, 124–132. [[CrossRef](#)] [[PubMed](#)]
48. Alauddin, M.M. Positron emission tomography (PET) imaging with (18)F-based radiotracers. *Am. J. Nucl. Med. Mol. Imaging* **2011**, *2*, 55–76. [[PubMed](#)]
49. Conti, M.; Eriksson, L. Physics of pure and non-pure positron emitters for PET: A review and a discussion. *EJNMMI Phys.* **2016**, *3*, 1–17. [[CrossRef](#)]
50. Jacobson, O.; Kieseewetter, D.O.; Chen, X. Fluorine-18 Radiochemistry, Labeling Strategies and Synthetic Routes. *Bioconjugate Chem.* **2015**, *26*, 1–18. [[CrossRef](#)]
51. Richter, S.; Wuest, F. ¹⁸F-Labeled Peptides: The Future Is Bright. *Molecules* **2014**, *19*, 20536–20556. [[CrossRef](#)]
52. Asti, M.; De Pietri, G.; Fraternali, A.; Grassi, E.; Sghedoni, R.; Fioroni, F.; Roesch, F.; Versari, A.; Salvo, D. Validation of ⁶⁸Ge/⁶⁸Ga generator processing by chemical purification for routine clinical application of ⁶⁸Ga-DOTATOC. *Nucl. Med. Biol.* **2008**, *35*, 721–724. [[CrossRef](#)]
53. Fani, M.; André, J.P.; Maecke, H.R. ⁶⁸Ga-PET: A powerful generator-based alternative to cyclotron-based PET radiopharmaceuticals. *Contrast Media Mol. Imaging* **2008**, *3*, 53–63. [[CrossRef](#)]
54. Müller, C.; Bunka, M.; Reber, J.; Fischer, C.; Zhernosekov, K.; Türler, A.; Schibli, R. Promises of Cyclotron-Produced ⁴⁴Sc as a Diagnostic Match for Trivalent β⁻-Emitters: In Vitro and In Vivo Study of a ⁴⁴Sc-DOTA-Folate Conjugate. *J. Nucl. Med.* **2013**, *54*, 2168–2174. [[CrossRef](#)] [[PubMed](#)]
55. Breeman, W.A.; de Blois, E.; Chan, H.S.; Konijnenberg, M.; Kwekkeboom, D.J.; Krenning, E.P. ⁶⁸Ga-labeled DOTA-Peptides and ⁶⁸Ga-labeled Radiopharmaceuticals for Positron Emission Tomography: Current Status of Research, Clinical Applications, and Future Perspectives. *Semin. Nucl. Med.* **2011**, *41*, 314–321. [[CrossRef](#)] [[PubMed](#)]
56. Gabriel, M.; Decristoforo, C.; Kandler, D.; Dobrozemsky, G.; Heute, D.; Uprimny, C.; Kovacs, P.; Von Guggenberg, E.; Bale, R.; Virgolini, I.J. ⁶⁸Ga-DOTA-Tyr3-Octreotide PET in Neuroendocrine Tumors: Comparison with Somatostatin Receptor Scintigraphy and CT. *J. Nucl. Med.* **2007**, *48*, 508–518. [[CrossRef](#)]
57. Roesch, F.; Riss, P.J. The Renaissance of the ⁶⁸Ge/⁶⁸Ga Radionuclide Generator Initiates New Developments in ⁶⁸Ga Radiopharmaceutical Chemistry. *Curr. Top. Med. Chem.* **2010**, *10*, 1633–1668. [[CrossRef](#)] [[PubMed](#)]
58. Fichna, J.; Janecka, A. Synthesis of Target-Specific Radiolabeled Peptides for Diagnostic Imaging. *Bioconjugate Chem.* **2003**, *14*, 3–17. [[CrossRef](#)]
59. McCarthy, D.W.; Shefer, R.E.; Klinkowstein, R.E.; Bass, L.A.; Margeneau, W.H.; Cutler, C.S.; Anderson, C.J.; Welch, M.J. Efficient production of high specific activity ⁶⁴Cu using a biomedical cyclotron. *Nucl. Med. Biol.* **1997**, *24*, 35–43. [[CrossRef](#)]
60. Anderson, C.J.; Ferdani, R. Copper-64 Radiopharmaceuticals for PET Imaging of Cancer: Advances in Preclinical and Clinical Research. *Cancer Biotherapy Radiopharm.* **2009**, *24*, 379–393. [[CrossRef](#)]
61. Holland, J.P.; Ferdani, R.; Anderson, C.J.; Lewis, J.S. Copper-64 Radiopharmaceuticals for Oncologic Imaging. *PET Clin.* **2009**, *4*, 49–67. [[CrossRef](#)]
62. Walczak, R.; Krajewski, S.; Szkliniarz, K.; Sitarz, M.; Abbas, K.; Choiński, J.; Jakubowski, A.; Jastrzębski, J.; Majkowska, A.; Simonelli, F.; et al. Cyclotron production of ⁴³Sc for PET imaging. *EJNMMI Phys.* **2015**, *2*, 33. [[CrossRef](#)]
63. Zhang, Y.; Hong, H.; Cai, W. PET Tracers Based on Zirconium-89. *Curr. Radiopharm.* **2011**, *4*, 131–139. [[CrossRef](#)]
64. de Ruijter, L.K.; Hooiveld-Noeken, J.S.; Giesen, D.; Hooge, M.N.L.-D.; Kok, I.C.; Brouwers, A.H.; Elias, S.G.; Nguyen, M.T.; Lu, H.; Gietema, J.A.; et al. First-in-Human Study of the Biodistribution and Pharmacokinetics of ⁸⁹Zr-CX-072, a Novel Immunopet Tracer Based on an Anti-PD-L1 Probody. *Clin. Cancer Res.* **2021**, *27*, 5325–5333. [[CrossRef](#)] [[PubMed](#)]
65. Mulgaonkar, A.; Elias, R.; Woolford, L.; Guan, B.; Nham, K.; Kapur, P.; Christie, A.; Tcheuyap, V.T.; Singla, N.; Bowman, I.A.; et al. ImmunoPET Imaging with ⁸⁹Zr-Labeled Atezolizumab Enables In Vivo Evaluation of PD-L1 in Tumorgraft Models of Renal Cell Carcinoma. *Clin. Cancer Res.* **2022**, *28*, 4907–4916. [[CrossRef](#)] [[PubMed](#)]
66. Dijkers, E.C.; Kosterink, J.G.; Rademaker, A.P.; Perk, L.R.; van Dongen, G.A.; Bart, J.; de Jong, J.R.; de Vries, E.G.; Lub-de Hooge, M.N. Development and Characterization of Clinical-Grade ⁸⁹Zr-Trastuzumab for HER2/neu ImmunoPET Imaging. *J. Nucl. Med.* **2009**, *50*, 974–981. [[CrossRef](#)] [[PubMed](#)]
67. Holland, J.P.; Divilov, V.; Bander, N.H.; Smith-Jones, P.M.; Larson, S.M.; Lewis, J.S. ⁸⁹Zr-DFO-J591 for ImmunoPET of Prostate-Specific Membrane Antigen Expression In Vivo. *J. Nucl. Med.* **2010**, *51*, 1293–1300. [[CrossRef](#)]
68. Nagengast, W.B.; De Vries, E.G.; Hospers, G.A.; Mulder, N.H.; De Jong, J.R.; Hollema, H.; Brouwers, A.H.; Van Dongen, G.A.; Perk, L.R.; Lub-de Hooge, M.N. In Vivo VEGF Imaging with Radiolabeled Bevacizumab in a Human Ovarian Tumor Xenograft. *J. Nucl. Med.* **2007**, *48*, 1313–1319. [[CrossRef](#)] [[PubMed](#)]
69. Perk, L.R.; Visser, G.W.M.; Vosjan, M.J.W.D.; Walsum, M.S.-V.; Tijink, B.M.; Leemans, C.R.; van Dongen, G.A.M.S. (⁸⁹Zr) as a PET surrogate radioisotope for scouting biodistribution of the therapeutic radiometals (⁹⁰Y) and (¹⁷⁷Lu) in tumor-bearing nude mice after coupling to the internalizing antibody cetuximab. *J. Nucl. Med.* **2005**, *46*, 1898–1906.
70. Deri, M.A.; Zeglis, B.M.; Francesconi, L.C.; Lewis, J.S. PET imaging with ⁸⁹Zr: From radiochemistry to the clinic. *Nucl. Med. Biol.* **2012**, *40*, 3–14. [[CrossRef](#)]
71. Verel, I.; Visser, G.W.M.; Boellaard, R.; Boerman, O.C.; Van Eerd, J.; Snow, G.B.; A Lammertsma, A.; van Dongen, G.A.M.S. Quantitative ⁸⁹Zr immuno-PET for in vivo scouting of ⁹⁰Y-labeled monoclonal antibodies in xenograft-bearing nude mice. *J. Nucl. Med.* **2003**, *44*, 1663–1670.

72. Zeglis, B.M.; Houghton, J.L.; Evans, M.J.; Viola, N.; Lewis, J.S. Underscoring the Influence of Inorganic Chemistry on Nuclear Imaging with Radiometals. *Inorg. Chem.* **2014**, *53*, 1880–1899. [[CrossRef](#)]
73. Alzimami, K.S.; Ma, A.K. Effective dose to staff members in a positron emission tomography/CT facility using zirconium-89. *Br. J. Radiol.* **2013**, *86*, 20130318. [[CrossRef](#)]
74. Vugts, D.J.; van Dongen, G.A. ⁸⁹Zr-labeled compounds for PET imaging guided personalized therapy. *Drug Discov. Today Technol.* **2011**, *8*, e53–e61. [[CrossRef](#)] [[PubMed](#)]
75. Kálmán-Szabó, I.; Szabó, J.P.; Arató, V.; Dénes, N.; Opposits, G.; Józai, I.; Kertész, I.; Képes, Z.; Fekete, A.; Szikra, D.; et al. PET Probes for Preclinical Imaging of GRPR-Positive Prostate Cancer: Comparative Preclinical Study of [⁶⁸Ga]Ga-NODAGA-AMBA and [⁴⁴Sc]Sc-NODAGA-AMBA. *Int. J. Mol. Sci.* **2022**, *23*, 10061. [[CrossRef](#)] [[PubMed](#)]
76. Domnanich, K.A.; Müller, C.; Farkas, R.; Schmid, R.M.; Ponsard, B.; Schibli, R.; Türlér, A.; van der Meulen, N.P. ⁴⁴Sc for labeling of DOTA- and NODAGA-functionalized peptides: Preclinical in vitro and in vivo investigations. *EJNMMI. Radiopharm. Chem.* **2017**, *1*, 8. [[CrossRef](#)] [[PubMed](#)]
77. Nagy, G.; Szikra, D.; Trencsényi, G.; Fekete, A.; Garai, I.; Giani, A.M.; Negri, R.; Masciocchi, N.; Maiocchi, A.; Uggeri, F.; et al. AAZTA: An Ideal Chelating Agent for the Development of ⁴⁴Sc PET Imaging Agents. *Angew. Chem. Int. Ed.* **2017**, *56*, 2118–2122. [[CrossRef](#)] [[PubMed](#)]
78. Szűcs, D.; Csupász, T.; Szabó, J.P.; Kis, A.; Gyuricza, B.; Arató, V.; Forgács, V.; Vágner, A.; Nagy, G.; Garai, I.; et al. Synthesis, Physicochemical, Labeling and In Vivo Characterization of ⁴⁴Sc-Labeled DO3AM-NI as a Hypoxia-Sensitive PET Probe. *Pharmaceuticals* **2022**, *15*, 666. [[CrossRef](#)]
79. Masłowska, K.; Redkiewicz, P.; Halik, P.K.; Witkowska, E.; Tymecka, D.; Walczak, R.; Chojiński, J.; Misicka, A.; Gniazdowska, E. Scandium-44 Radiolabeled Peptide and Peptidomimetic Conjugates Targeting Neuropilin-1 Co-Receptor as Potential Tools for Cancer Diagnosis and Anti-Angiogenic Therapy. *Biomedicines* **2023**, *11*, 564. [[CrossRef](#)]
80. Wilder, R.L. Integrin alpha V beta 3 as a target for treatment of rheumatoid arthritis and related rheumatic diseases. *Ann. Rheum. Dis.* **2002**, *61* (Suppl. S2), 96–99. [[CrossRef](#)]
81. Eble, J.A.; Haier, J.A.E.A.J. Integrins in Cancer Treatment. *Curr. Cancer Drug Targets* **2006**, *6*, 89–105. [[CrossRef](#)]
82. Liu, Z.; Wang, F.; Chen, X. Integrin $\alpha_v\beta_3$ -targeted cancer therapy. *Drug Dev. Res.* **2008**, *69*, 329–339. [[CrossRef](#)]
83. Kumar, C.C. Integrin $\alpha_v\beta_3$ as a Therapeutic Target for Blocking Tumor-Induced Angiogenesis. *Curr. Drug Targets* **2003**, *4*, 123–131. [[CrossRef](#)]
84. A Schwartz, M. Integrin signaling revisited. *Trends Cell Biol.* **2001**, *11*, 466–470. [[CrossRef](#)] [[PubMed](#)]
85. Chen, H.; Niu, G.; Wu, H.; Chen, X. Clinical Application of Radiolabeled RGD Peptides for PET Imaging of Integrin $\alpha_v\beta_3$. *Theranostics* **2016**, *6*, 78–92. [[CrossRef](#)] [[PubMed](#)]
86. Glaser, M.; Morrison, M.; Solbakken, M.; Arukwe, J.; Karlsen, H.; Wiggen, U.; Champion, S.; Kindberg, G.M.; Cuthbertson, A. Radiosynthesis and Biodistribution of Cyclic RGD Peptides Conjugated with Novel [¹⁸F]Fluorinated Aldehyde-Containing Prosthetic Groups. *Bioconjugate Chem.* **2008**, *19*, 951–957. [[CrossRef](#)] [[PubMed](#)]
87. Haubner, R.; Weber, W.A.; Beer, A.J.; Vabulienė, E.; Reim, D.; Sarbia, M.; Becker, K.-F.; Goebel, M.; Hein, R.; Wester, H.-J.; et al. Noninvasive Visualization of the Activated $\alpha_v\beta_3$ Integrin in Cancer Patients by Positron Emission Tomography and [¹⁸F]Galacto-RGD. *PLoS Med.* **2005**, *2*, e70. [[CrossRef](#)] [[PubMed](#)]
88. Kolb, H.; Walsh, J.; Walsh, J.; Chen, G.; Gangadharmath, U.; Kasi, D.; Scott, P.; Haka, M.; Collier, T.; Padgett, H. Synthesis of an ¹⁸F-labeled RGD peptide for imaging $\alpha_v\beta_3$ integrin expression in vivo. *J. Nucl. Med.* **2009**, *50*, 1939.
89. Lang, L.; Li, W.; Guo, N.; Ma, Y.; Zhu, L.; Kiesewetter, D.O.; Shen, B.; Niu, G.; Chen, X. Comparison Study of [¹⁸F]FAI-NOTA-PRGD2, [¹⁸F]FPPRGD2, and [⁶⁸Ga]Ga-NOTA-PRGD2 for PET Imaging of U87MG Tumors in Mice. *Bioconjugate Chem.* **2011**, *22*, 2415–2422. [[CrossRef](#)]
90. Liu, S.; Liu, Z.; Chen, K.; Yan, Y.; Watzlowik, P.; Wester, H.-J.; Chin, F.T.; Chen, X. ¹⁸F-Labeled Galacto and PEGylated RGD Dimers for PET Imaging of $\alpha_v\beta_3$ Integrin Expression. *Mol. Imaging Biol.* **2010**, *12*, 530–538. [[CrossRef](#)]
91. Kim, J.H.; Lee, J.S.; Kang, K.W.; Lee, H.-Y.; Han, S.-W.; Kim, T.-Y.; Lee, Y.-S.; Jeong, J.M.; Lee, D.S. Whole-Body Distribution and Radiation Dosimetry of ⁶⁸Ga-NOTA-RGD, a Positron Emission Tomography Agent for Angiogenesis Imaging. *Cancer Biotherapy Radiopharm.* **2012**, *27*, 65–71. [[CrossRef](#)]
92. Zheng, K.; Liang, N.; Zhang, J.; Lang, L.; Zhang, W.; Li, S.; Zhao, J.; Niu, G.; Li, F.; Zhu, Z.; et al. ⁶⁸Ga-NOTA-PRGD2 PET/CT for Integrin Imaging in Patients with Lung Cancer. *J. Nucl. Med.* **2015**, *56*, 1823–1827. [[CrossRef](#)]
93. Liapis, H.; Flath, A.; Kitazawa, S. Integrin $\alpha_v\beta_3$ Expression by Bone-residing Breast Cancer Metastases. *Diagn. Mol. Pathol.* **1996**, *5*, 127–135. [[CrossRef](#)]
94. Ghiani, S.; Hawala, I.; Szikra, D.; Trencsényi, G.; Baranyai, Z.; Nagy, G.; Vágner, A.; Stefania, R.; Pandey, S.; Maiocchi, A. Synthesis, radiolabeling, and pre-clinical evaluation of [⁴⁴Sc]Sc-AAZTA conjugate PSMA inhibitor, a new tracer for high-efficiency imaging of prostate cancer. *Eur. J. Nucl. Med.* **2021**, *48*, 2351–2362. [[CrossRef](#)] [[PubMed](#)]
95. Asti, M.; Iori, M.; Capponi, P.C.; Atti, G.; Rubagotti, S.; Martin, R.; Brennauer, A.; Müller, M.; Bergmann, R.; Erba, P.A.; et al. Influence of different chelators on the radiochemical properties of a ⁶⁸Gallium labelled bombesin analogue. *Nucl. Med. Biol.* **2014**, *41*, 24–35. [[CrossRef](#)] [[PubMed](#)]
96. Bartholdi, M.F.; Wu, J.M.; Pu, H.; Troncoso, P.; Eden, P.A.; Feldman, R.I. In situ hybridization for gastrin-releasing peptide receptor (GRP receptor) expression in prostatic carcinoma. *Int. J. Cancer* **1998**, *79*, 82–90. [[CrossRef](#)]

97. Chave, H.S.; Gough, A.C.; Palmer, K.; Preston, S.R.; Primrose, J.N. Bombesin family receptor and ligand gene expression in human colorectal cancer and normal mucosa. *Br. J. Cancer* **2000**, *82*, 124–130. [[CrossRef](#)]
98. Fleischmann, A.; Läderach, U.; Friess, H.; Buechler, M.W.; Reubi, J.C. Bombesin Receptors in Distinct Tissue Compartments of Human Pancreatic Diseases. *Lab. Investig.* **2000**, *80*, 1807–1817. [[CrossRef](#)]
99. Halmos, G.; Wittliff, J.L.; Schally, A.V. Characterization of bombesin/gastrin-releasing peptide receptors in human breast cancer and their relationship to steroid receptor expression. *Cancer Res.* **1995**, *55*, 280–287.
100. Markwalder, R.; Reubi, J.C. Gastrin-releasing peptide receptors in the human prostate: Relation to neoplastic transformation. *Cancer Res.* **1999**, *59*, 1152–1159.
101. Mattei, J.; Achcar, R.D.; Cano, C.H.; Macedo, B.R.; Meurer, L.; Batlle, B.S.; Groshong, S.D.; Kulczynski, J.M.; Roesler, R.; Lago, L.D.; et al. Gastrin-Releasing Peptide Receptor Expression in Lung Cancer. *Arch. Pathol. Lab. Med.* **2014**, *138*, 98–104. [[CrossRef](#)]
102. Reubi, J.C. Peptide Receptors as Molecular Targets for Cancer Diagnosis and Therapy. *Endocr. Rev.* **2003**, *24*, 389–427. [[CrossRef](#)]
103. Fleischmann, A.; Waser, B.; Reubi, J.C. Overexpression of Gastrin-Releasing Peptide Receptors in Tumor-Associated Blood Vessels of Human Ovarian Neoplasms. *Anal. Cell. Pathol.* **2007**, *29*, 421–433. [[CrossRef](#)]
104. Elshafae, S.M.; Hassan, B.B.; Supsavhad, W.; Dirksen, W.P.; Camiener, R.Y.; Ding, H.; Tweedle, M.F.; Rosol, T.J. Gastrin-releasing peptide receptor (GRPr) promotes EMT, growth, and invasion in canine prostate cancer. *Prostate* **2016**, *76*, 796–809. [[CrossRef](#)] [[PubMed](#)]
105. Jensen, R.T.; Moody, T.; Pert, C.; Rivier, J.E.; Gardner, J.D. Interaction of bombesin and litorin with specific membrane receptors on pancreatic acinar cells. *Proc. Natl. Acad. Sci. USA* **1978**, *75*, 6139–6143. [[CrossRef](#)] [[PubMed](#)]
106. Oliveira-Freitas, V.L.; Thomaz, L.D.G.R.; Simoneti, L.E.L.; Malfitano, C.; De Angelis, K.; Ulbrich, J.M.; Schwartzmann, G.; Andrade, C.F. RC-3095, a Selective Gastrin-Releasing Peptide Receptor Antagonist, Does Not Protect the Lungs in an Experimental Model of Lung Ischemia-Reperfusion Injury. *Biomed. Res. Int.* **2015**, *2015*, 496378. [[CrossRef](#)] [[PubMed](#)]
107. Bajo, A.M.; Schally, A.V.; Groot, K.; Szepeshazi, K. Bombesin antagonists inhibit proangiogenic factors in human experimental breast cancers. *Br. J. Cancer* **2004**, *90*, 245–252. [[CrossRef](#)]
108. Heuser, M.; Schlott, T.; Schally, A.; Kahler, E.; Schliephake, R.; Laabs, S.; Hemmerlein, B. Expression of gastrin releasing peptide receptor in renal cell carcinomas: A potential function for the regulation of neoangiogenesis and microvascular perfusion. *J. Urol.* **2005**, *173*, 2154–2159. [[CrossRef](#)]
109. Kanashiro, C.A.; Schally, A.; Cai, R.-Z.; Halmos, G. Antagonists of bombesin/gastrin-releasing peptide decrease the expression of angiogenic and anti-apoptotic factors in human glioblastoma. *Anti-Cancer Drugs* **2005**, *16*, 159–165. [[CrossRef](#)]
110. Levine, L.; Lucci, J.A., III; Pazdrak, B.; Cheng, J.Z.; Guo, Y.S.; Townsend, C.M., Jr.; Hellmich, M.R. Bombesin stimulates nuclear factor KB activation and expression of proangiogenic factors in prostate cancer cells. *Cancer Res.* **2003**, *63*, 3495–3502.
111. Reile, H.; Armatis, P.E.; Schally, A.V. Characterization of high-affinity receptors for bombesin/gastrin releasing peptide on the human prostate cancer cell lines PC-3 and DU-145: Internalization of receptor bound ¹²⁵I-(Tyr⁴) bombesin by tumor cells. *Prostate* **1994**, *25*, 29–38. [[CrossRef](#)]
112. Hennessy, B.T.; Smith, D.L.; Ram, P.T.; Lu, Y.; Mills, G.B. Exploiting the PI3K/AKT Pathway for Cancer Drug Discovery. *Nat. Rev. Drug Discov.* **2005**, *4*, 988–1004. [[CrossRef](#)]
113. Kang, J.; Ishola, T.A.; Baregamian, N.; Mourot, J.M.; Rychahou, P.G.; Evers, B.M.; Chung, D.H. Bombesin induces angiogenesis and neuroblastoma growth. *Cancer Lett.* **2007**, *253*, 273–281. [[CrossRef](#)]
114. Katso, R.; Okkenhaug, K.; Ahmadi, K.; White, S.; Timms, J.; Waterfield, M.D. Cellular Function of Phosphoinositide 3-Kinases: Implications for Development, Immunity, Homeostasis, and Cancer. *Annu. Rev. Cell Dev. Biol.* **2001**, *17*, 615–675. [[CrossRef](#)] [[PubMed](#)]
115. E Lantry, L.; Cappelletti, E.; Maddalena, M.E.; Fox, J.S.; Feng, W.; Chen, J.; Thomas, R.; Eaton, S.M.; Bogdan, N.J.; Arunachalam, T.; et al. ¹⁷⁷Lu-AMBA: Synthesis and characterization of a selective ¹⁷⁷Lu-labeled GRP-R agonist for systemic radiotherapy of prostate cancer. *J. Nucl. Med.* **2006**, *47*, 1144–1152.
116. Liu, Y.; Hu, X.; Liu, H.; Bu, L.; Ma, X.; Cheng, K.; Li, J.; Tian, M.; Zhang, H.; Cheng, Z. A Comparative Study of Radiolabeled Bombesin Analogs for the PET Imaging of Prostate Cancer. *J. Nucl. Med.* **2013**, *54*, 2132–2138. [[CrossRef](#)] [[PubMed](#)]
117. Schroeder, R.P.J.; Müller, C.; Reneman, S.; Melis, M.L.; Breeman, W.A.P.; de Blois, E.; Bangma, C.H.; Krenning, E.P.; van Weerden, W.M.; de Jong, M. A standardised study to compare prostate cancer targeting efficacy of five radiolabelled bombesin analogues. *Eur. J. Nucl. Med.* **2010**, *37*, 1386–1396. [[CrossRef](#)] [[PubMed](#)]
118. Bologna, M.; Festuccia, C.; Muzi, P.; Biordi, L.; Ciomei, M. Bombesin Stimulates Growth of Human Prostatic Cancer Cells in Vitro. *Cancer* **1989**, *63*, 1714–1720. [[CrossRef](#)]
119. Kilgore, W.; Mantyh, P.; Mantyh, C.; McVey, D.; Vigna, S. Bombesin/GRP-preferring and neuromedin B-preferring receptors in the rat urogenital system. *Neuropeptides* **1993**, *24*, 43–52. [[CrossRef](#)]
120. Jensen, R.T.; Batey, J.F.; Spindel, E.R.; Benya, R.V. International Union of Pharmacology. LXVIII. Mammalian Bombesin Receptors: Nomenclature, Distribution, Pharmacology, Signaling, and Functions in Normal and Disease States. *Pharmacol. Rev.* **2008**, *60*, 1–42. [[CrossRef](#)]
121. Johnson, D.E.; Georgieff, M.K. Pulmonary Neuroendocrine Cells: Their Secretory Products and Their Potential Roles in Health and Chronic Lung Disease in Infancy. *Am. Rev. Respir. Dis.* **1989**, *140*, 1807–1812. [[CrossRef](#)]

122. Weber, H.C. Regulation and signaling of human bombesin receptors and their biological effects. *Curr. Opin. Endocrinol. Diabetes* **2009**, *16*, 66–71. [[CrossRef](#)]
123. Smith, C.; Volkert, W.; Hoffman, T. Gastrin releasing peptide (GRP) receptor targeted radiopharmaceuticals: A concise update. *Nucl. Med. Biol.* **2003**, *30*, 861–868. [[CrossRef](#)]
124. Barthel, H.; Wilson, H.; Collingridge, D.R.; Brown, G.; Osman, S.; Luthra, S.K.; Brady, F.; Workman, P.; Price, P.M.; Aboagye, E. In vivo evaluation of [¹⁸F]fluoroetanidazole as a new marker for imaging tumour hypoxia with positron emission tomography. *Br. J. Cancer* **2004**, *90*, 2232–2242. [[CrossRef](#)] [[PubMed](#)]
125. Yang, D.J.; Wallace, S.; Cherif, A.; Li, C.; Gretzer, M.B.; E Kim, E.; A Podoloff, D. Development of F-18-labeled fluoroerythronitroimidazole as a PET agent for imaging tumor hypoxia. *Radiology* **1995**, *194*, 795–800. [[CrossRef](#)] [[PubMed](#)]
126. Ziemer, L.; Evans, S.; Kachur, A.; Shuman, A.; Cardi, C.; Jenkins, W.; Karp, J.; Alavi, A.; Dolbier, W.; Koch, C. Noninvasive imaging of tumor hypoxia in rats using the 2-nitroimidazole 18F-EF5. *Eur. J. Nucl. Med.* **2003**, *30*, 259–266. [[CrossRef](#)] [[PubMed](#)]
127. Ferrara, N.; Kerbel, R.S. Angiogenesis as a therapeutic target. *Nature* **2005**, *438*, 967–974. [[CrossRef](#)]
128. Gray, L.H.; Conger, A.D.; Ebert, M.; Hornsey, S.; Scott, O.C.A. The Concentration of Oxygen Dissolved in Tissues at the Time of Irradiation as a Factor in Radiotherapy. *Br. J. Radiol.* **1953**, *26*, 638–648. [[CrossRef](#)]
129. Semenza, G.L. HIF-1 and tumor progression: Pathophysiology and therapeutics. *Trends Mol. Med.* **2002**, *8*, S62–S67. [[CrossRef](#)]
130. Sun, X.; Niu, G.; Chan, N.; Shen, B.; Chen, X. Tumor Hypoxia Imaging. *Mol. Imaging Biol.* **2011**, *13*, 399–410. [[CrossRef](#)]
131. Koh, W.-J.; Rasey, J.S.; Evans, M.L.; Grierson, J.R.; Lewellen, T.K.; Graham, M.; Krohn, K.A.; Griffin, T.W. Imaging of hypoxia in human tumors with [F-18]fluoromisonidazole. *Int. J. Radiat. Oncol.* **1992**, *22*, 199–212. [[CrossRef](#)]
132. Reischl, G.; Ehrlichmann, W.; Bieg, C.; Solbach, C.; Kumar, P.; Wiebe, L.I.; Machulla, H.-J. Preparation of the hypoxia imaging PET tracer [¹⁸F]FAZA: Reaction parameters and automation. *Appl. Radiat. Isot.* **2005**, *62*, 897–901. [[CrossRef](#)]
133. Hoigebazar, L.; Jeong, J.M.; Hong, M.K.; Kim, Y.J.; Lee, J.Y.; Shetty, D.; Lee, Y.-S.; Lee, D.S.; Chung, J.-K.; Lee, M.C. Synthesis of ⁶⁸Ga-labeled DOTA-nitroimidazole derivatives and their feasibilities as hypoxia imaging PET tracers. *Bioorganic Med. Chem.* **2011**, *19*, 2176–2181. [[CrossRef](#)]
134. Cherif, A.; Wallace, S.; Yang, D.; Newman, R.; Harrod, V.; Nornoo, A.; Inoue, T.; Kim, C.; Kuang, L.-R.; Kim, E.; et al. Development of new markers for hypoxic cells: [¹³¹I]Iodomisonidazole and [¹³¹I]Iodoerythronitroimidazole. *J. Drug Target.* **1996**, *4*, 31–39. [[CrossRef](#)] [[PubMed](#)]
135. Liu, R.-S.; Chou, T.-K.; Chang, C.-H.; Wu, C.-Y.; Chang, C.-W.; Chang, T.-J.; Wang, S.-J.; Lin, W.-J.; Wang, H.-E. Biodistribution, pharmacokinetics and PET Imaging of [¹⁸F]FMISO, [¹⁸F]FDG and [¹⁸F]FAC in a sarcoma- and inflammation-bearing mouse model. *Nucl. Med. Biol.* **2009**, *36*, 305–312. [[CrossRef](#)] [[PubMed](#)]
136. Luo, Z.; Zhu, H.; Lin, X.; Chu, T.; Luo, R.; Wang, Y.; Yang, Z. Synthesis and radiolabeling of ⁶⁴Cu-labeled 2-nitroimidazole derivative ⁶⁴Cu-BMS2P2 for hypoxia imaging. *Bioorganic Med. Chem. Lett.* **2016**, *26*, 1397–1400. [[CrossRef](#)] [[PubMed](#)]
137. Sharma, R. Nitroimidazole radiopharmaceuticals in bioimaging: Part I: Synthesis and imaging applications. *Curr. Radiopharm.* **2011**, *4*, 361–378. [[CrossRef](#)] [[PubMed](#)]
138. Hoigebazar, L.; Jeong, J.M.; Choi, S.Y.; Choi, J.Y.; Shetty, D.; Lee, Y.-S.; Lee, D.S.; Chung, J.-K.; Lee, M.C.; Chung, Y.K. Synthesis and Characterization of Nitroimidazole Derivatives for ⁶⁸Ga-Labeling and Testing in Tumor Xenografted Mice. *J. Med. Chem.* **2010**, *53*, 6378–6385. [[CrossRef](#)] [[PubMed](#)]
139. Seelam, S.R.; Lee, J.Y.; Lee, Y.-S.; Hong, M.K.; Kim, Y.J.; Banka, V.K.; Lee, D.S.; Chung, J.-K.; Jeong, J.M. Development of ⁶⁸Ga-labeled multivalent nitroimidazole derivatives for hypoxia imaging. *Bioorganic Med. Chem.* **2015**, *23*, 7743–7750. [[CrossRef](#)]
140. Jussila, L.; Alitalo, K. Vascular Growth Factors and Lymphangiogenesis. *Physiol. Rev.* **2002**, *82*, 673–700. [[CrossRef](#)]
141. Takahashi, H.; Shibuya, M. The vascular endothelial growth factor (VEGF)/VEGF receptor system and its role under physiological and pathological conditions. *Clin. Sci.* **2005**, *109*, 227–241. [[CrossRef](#)]
142. Djordjevic, S.; Driscoll, P.C. Targeting VEGF signalling via the neuropilin co-receptor. *Drug Discov. Today* **2013**, *18*, 447–455. [[CrossRef](#)]
143. E Bachelder, R.; Crago, A.; Chung, J.; A Wendt, M.; Shaw, L.M.; Robinson, G.; Mercurio, A.M. Vascular endothelial growth factor is an autocrine survival factor for neuropilin-expressing breast carcinoma cells. *Cancer Res.* **2001**, *61*, 5736–5740.
144. Cao, Y.; Wang, L.; Nandy, D.; Zhang, Y.; Basu, A.; Radisky, D.; Mukhopadhyay, D. Neuropilin-1 Upholds Dedifferentiation and Propagation Phenotypes of Renal Cell Carcinoma Cells by Activating Akt and Sonic Hedgehog Axes. *Cancer Res* **2008**, *68*, 8667–8672. [[CrossRef](#)] [[PubMed](#)]
145. Hamerlik, P.; Lathia, J.D.; Rasmussen, R.; Wu, Q.; Bartkova, J.; Lee, M.; Moudry, P.; Bartek, J., Jr.; Fischer, W.; Lukas, J.; et al. Autocrine VEGF-VEGFR2-Neuropilin-1 signaling promotes glioma stem-like cell viability and tumor growth. *J. Exp. Med.* **2012**, *209*, 507–520. [[CrossRef](#)] [[PubMed](#)]
146. Hong, T.-M.; Chen, Y.-L.; Wu, Y.-Y.; Yuan, A.; Chao, Y.-C.; Chung, Y.-C.; Wu, M.-H.; Yang, S.-C.; Pan, S.-H.; Shih, J.-Y.; et al. Targeting Neuropilin 1 as an Antitumor Strategy in Lung Cancer. *Clin. Cancer Res.* **2007**, *13*, 4759–4768. [[CrossRef](#)] [[PubMed](#)]
147. Peng, K.; Bai, Y.; Zhu, Q.; Hu, B.; Xu, Y. Targeting VEGF-neuropilin interactions: A promising antitumor strategy. *Drug Discov. Today* **2019**, *24*, 656–664. [[CrossRef](#)] [[PubMed](#)]
148. Wickström, M.; Larsson, R.; Nygren, P.; Gullbo, J. Aminopeptidase N (CD13) as a target for cancer chemotherapy. *Cancer Sci.* **2011**, *102*, 501–508. [[CrossRef](#)] [[PubMed](#)]
149. Mina-Osorio, P. The moonlighting enzyme CD13: Old and new functions to target. *Trends Mol. Med.* **2008**, *14*, 361–371. [[CrossRef](#)]

150. Ito, S.; Miyahara, R.; Takahashi, R.; Nagai, S.; Takenaka, K.; Wada, H.; Tanaka, F. Stromal aminopeptidase N expression: Correlation with angiogenesis in non-small-cell lung cancer. *Gen. Thorac. Cardiovasc. Surg.* **2009**, *57*, 591–598. [[CrossRef](#)]
151. Sledge, G.W.; Rugo, H.S.; Burstein, H.J. The role of angiogenesis inhibition in the treatment of breast cancer. *Clin. Adv. Hematol. Oncol.* **2006**, *4*, 1–10.
152. Wang, X.; Niu, Z.; Jia, Y.; Cui, M.; Han, L.; Zhang, Y.; Liu, Z.; Bi, D.; Liu, S. Ubenimex inhibits cell proliferation, migration and invasion by inhibiting the expression of APN and inducing autophagic cell death in prostate cancer cells. *Oncol. Rep.* **2016**, *35*, 2121–2130. [[CrossRef](#)]
153. Pasqualini, R.; Koivunen, E.; Kain, R.; Lahdenranta, J.; Sakamoto, M.; Stryhn, A.; Ashmun, R.A.; Shapiro, L.H.; Arap, W.; Ruoslahti, E. Aminopeptidase N is a receptor for tumor-homing peptides and a target for inhibiting angiogenesis. *Cancer Res.* **2000**, *60*, 722–727.
154. Corti, A. Tumor Vasculature Targeting Through NGR Peptide-Based Drug Delivery Systems. *Curr. Pharm. Biotechnol.* **2011**, *12*, 1128–1134. [[CrossRef](#)] [[PubMed](#)]
155. Dijkgraaf, I.; Van de Vijver, P.; Dirksen, A.; Hackeng, T.M. Synthesis and application of cNGR-containing imaging agents for detection of angiogenesis. *Bioorganic Med. Chem.* **2013**, *21*, 3555–3564. [[CrossRef](#)] [[PubMed](#)]
156. Zhu, L.; Ding, Z.; Li, X.; Wei, H.; Chen, Y. Research Progress of Radiolabeled Asn-Gly-Arg (NGR) Peptides for Imaging and Therapy. *Mol. Imaging* **2020**, *19*, 1536012120934957. [[CrossRef](#)] [[PubMed](#)]
157. Gyuricza, B.; Szabó, J.P.; Arató, V.; Dénes, N.; Szűcs, Á.; Berta, K.; Kis, A.; Szűcs, D.; Forgács, V.; Szikra, D.; et al. Synthesis of ⁶⁸Ga-Labeled cNGR-Based Glycopeptides and In Vivo Evaluation by PET Imaging. *Pharmaceutics* **2021**, *13*, 2103. [[CrossRef](#)] [[PubMed](#)]
158. Kis, A.; Dénes, N.; Szabó, J.P.; Arató, V.; Józai, I.; Enyedi, K.N.; Lakatos, S.; Garai, I.; Mező, G.; Kertész, I.; et al. In vivo assessment of aminopeptidase N (APN/CD13) specificity of different ⁶⁸Ga-labelled NGR derivatives using PET/MRI imaging. *Int. J. Pharm.* **2020**, *589*, 119881. [[CrossRef](#)] [[PubMed](#)]
159. Máté, G.; Kertész, I.; Enyedi, K.N.; Mező, G.; Angyal, J.; Vasas, N.; Kis, A.; Szabó, É.; Emri, M.; Bíró, T.; et al. In vivo imaging of Aminopeptidase N (CD13) receptors in experimental renal tumors using the novel radiotracer ⁶⁸Ga-NOTA-c(NGR). *Eur. J. Pharm. Sci.* **2015**, *69*, 61–71. [[CrossRef](#)] [[PubMed](#)]
160. Li, G.; Wang, X.; Zong, S.; Wang, J.; Conti, P.S.; Chen, K. MicroPET Imaging of CD13 Expression Using a ⁶⁴Cu-Labeled Dimeric NGR Peptide Based on Sarcophagine Cage. *Mol. Pharm.* **2014**, *11*, 3938–3946. [[CrossRef](#)]
161. Ma, W.; Shao, Y.; Yang, W.; Li, G.; Zhang, Y.; Zhang, M.; Zuo, C.; Chen, K.; Wang, J. Evaluation of ¹⁸⁸Re-labeled NGR-VEGI protein for radioimaging and radiotherapy in mice bearing human fibrosarcoma HT-1080 xenografts. *Tumor Biol.* **2016**, *37*, 9121–9129. [[CrossRef](#)]
162. Vats, K.; Satpati, A.K.; Sharma, R.; Sarma, H.D.; Satpati, D.; Dash, A. ¹⁷⁷Lu-labeled cyclic Asn-Gly-Arg peptide tagged carbon nanospheres as tumor targeting radio-nanoprobes. *J. Pharm. Biomed. Anal.* **2018**, *152*, 173–178. [[CrossRef](#)]

Disclaimer/Publisher’s Note: The statements, opinions and data contained in all publications are solely those of the individual author(s) and contributor(s) and not of MDPI and/or the editor(s). MDPI and/or the editor(s) disclaim responsibility for any injury to people or property resulting from any ideas, methods, instructions or products referred to in the content.